Journal of Neuroscience Research 87:2498–2508 (2009)

Mechanism Underlying Apolipoprotein E (ApoE) Isoform-dependent Lipid Efflux From Neural Cells in Culture

Hirohisa Minagawa,[1] Jiang-Sheng Gong,[1] Cha-Gyun Jung,[1] Atsushi Watanabe,[2] Sissel Lund-Katz,[3] Michael C. Phillips,[3] Hiroyuki Saito,[4] and Makoto Michikawa[1]*

[1]Department of Alzheimer's Disease Research, National Institute for Longevity Sciences, National Center for Geriatrics and Gerontology, Aichi, Japan
[2]Department of Vascular Dementia, National Institute for Longevity Sciences, National Center for Geriatrics and Gerontology, Aichi, Japan
[3]Lipid Research Group, Children's Hospital of Philadelphia, University of Pennsylvania School of Medicine, Philadelphia, Pennsylvania
[4]Department of Biophysical Chemistry, Kobe Pharmaceutical University, Kobe, Japan

We determined the molecular mechanisms underlying apolipoprotein E (ApoE)-isoform-dependent lipid efflux from neurons and ApoE-deficient astrocytes in culture. The ability of ApoE3 to induce lipid efflux was 2.5- to 3.9-fold greater than ApoE4. To explore the contributions of the amino- and carboxyl-terminal tertiary structure domains of ApoE to cellular lipid efflux, each domain was studied separately. The amino-terminal fragment of ApoE3 (22-kDa-ApoE3) induced lipid efflux greater than 22-kDa-ApoE4, whereas the common carboxyl-terminal fragment of ApoE induced very low levels of lipid efflux. Addition of segments of the carboxyl-terminal domain to 22-kDa-ApoE3 additively induced lipid efflux in a length-dependent manner; in contrast, this effect did not occur with ApoE4. This observation, coupled with the fact that introduction of the E255A mutation (which disrupts domain–domain interaction) into ApoE4 increases lipid efflux, indicates that interaction between the amino- and carboxyl-terminal domains in ApoE4 reduces the ability of this isoform to mediate lipid efflux from neural cells. Dimeric 22-kDa or intact ApoE3 induced higher lipid efflux than monomeric 22-kDa or intact ApoE3, respectively, indicating that dimerization of ApoE3 enhances the ability to release lipids. The adenosine triphosphate–binding cassette protein A1 (ABCA1) is involved in ApoE-induced lipid efflux. In conclusion, there are two major factors, intramolecular domain interaction and intermolecular dimerization, that cause ApoE-isoform-dependent lipid efflux from neural cells in culture.

Key words: Alzheimer's disease; apolipoprotein E; high-density lipoprotein (HDL); neurons; astrocyte

The lipoprotein found in the central nervous system (CNS) is the high-density lipoprotein (HDL), and apolipoprotein E (ApoE) is one of the major apolipoproteins regulating lipid transport in CNS (Roheim et al., 1979; Pitas et al., 1987b; Weisgraber et al., 1994). Astrocytes and microglia synthesize and secrete ApoE (Boyles et al., 1985; Nakai et al., 1996), which interacts with adenosine triphosphate (ATP)-binding cassette protein A1 (ABCA1) (Krimbou et al., 2004) to remove cholesterol from cells and generate HDL particles in the cerebrospinal fluid and cultured media (Pitas et al., 1987a; Borghini et al., 1995; LaDu et al., 1998).

ApoE-inducible lipid efflux is ApoE-isoform dependent (Michikawa et al., 2000; Gong et al., 2002; Xu et al., 2004), and ApoE3 generates a similar number of HDL particles to but with a smaller number of ApoE molecules than ApoE4 (Gong et al., 2002). HDL synthesis mediated by ApoE contributes to cholesterol release from the cell membrane. On the other hand, HDL associated with ApoE is taken up by cells via ApoE receptors and the cholesterol in HDL is used for maintaining cholesterol homeostasis in CNS neurons. Thus, this isoform-specific action of ApoE to remove cholesterol and

Contract grant sponsor: Ministry of Health, Labor and Welfare of Japan (Research on Human Genome and Tissue Engineering); Contract grant number: H17-004; Contract grant sponsor: Program for Promotion of Fundamental Studies in Health of the National Institute of Biomedical Innovation (NIBIO); Contract grant sponsor: Japan Society for the Promotion of Science (JSPS); Contract grant sponsor: Naito Foundation; Contract grant sponsor: Grant-in-Aid for Scientific Research on Priority Areas—Research on Pathomechanisms of Brain Disorders, from the Ministry of Education, Culture, Sports, Science and Technology of Japan; Contract grant number: 18023046; Contract grant sponsor: NIH; Contract grant number: HL 56083.

*Correspondence to: Makoto Michikawa, Department of Alzheimer's Disease Research, National Institute for Longevity Sciences (NILS), National Center for Geriatrics and Gerontology (NCGG), 36-3 Gengo, Morioka, Obu, Aichi 474-8522, Japan. E-mail: michi@nils.go.jp

Received 30 September 2008; Revised 27 January 2009; Accepted 8 February 2009

Published online 26 March 2009 in Wiley InterScience (www.interscience.wiley.com). DOI: 10.1002/jnr.22073

generate HDL may be the cause of altered cholesterol metabolism in an Alzheimer's disease (AD) brain (Demeester et al., 2000; Molander-Melin et al., 2005) and may explain how ApoE4 serves as a strong risk factor for AD development (Corder et al., 1993; Strittmatter et al., 1993). However, the molecular mechanism underlying ApoE-isoform-dependent HDL generation remains to be elucidated.

The ApoE molecule has two distinct domains, namely, the 22-kDa amino-terminal (residues 1–191) and 10-kDa carboxyl-terminal domains (residue 218–299), that unfold independently of each other (Wetterau et al., 1988; Morrow et al., 2000). It has been demonstrated that ApoE4 amino- and carboxyl-domain interaction is responsible for the ApoE-isoform dependent association with lipid particles (Weisgraber, 1990; Dong and Weisgraber, 1996; Saito et al., 2003). The domain interaction in ApoE4 under physiological conditions has also been confirmed at the cellular level (Xu et al., 2004) and in vivo (Raffai et al., 2001; Ramaswamy et al., 2005), suggesting that the presence or absence of the domain interaction can explain ApoE-isoform dependent lipid efflux. In addition, there are ApoE-isoform dependent differences in the structure and stability of the 22-kDa amino-terminal fragment (22-kDa-ApoE), which affect their binding affinities to lipids (Morrow et al., 2000, 2002; Segall et al., 2002; Hatters et al., 2005), suggesting that the 22-kDa-ApoE that lacks the domain interaction may also explain an isoform-dependent lipid efflux.

In this study, we investigated the molecular mechanisms, by which intact ApoE3 has a greater ability to induce cholesterol efflux than intact-ApoE4 by using cultured rat neurons and astrocytes prepared from ApoE knockout mouse brain to exclude the effect of endogenously generated and secreted ApoE. We found that the intramolecular amino- and carboxyl-terminal domain interaction is partially responsible for this ApoE-isoform dependency. To our surprise, 22-kDa-ApoE3 has a greater ability to induce cholesterol efflux than 22-kDa-ApoE4. This is because 22-kDa-ApoE3 forms dimers, whereas 22-kDa-ApoE4 does not. These findings suggest that cholesterol efflux induced by ApoE is regulated by two major factors: the presence or absence of intermolecular dimer formation and the intramolecular domain interaction.

EXPERIMENTAL PROCEDURES

Cell Culture

All experiments were performed in compliance with existing laws and institutional guidelines. Neuron-rich cultures were prepared from rat cerebral cortices as previously described (Michikawa et al., 2001). Cerebral cortices from rat brains were dissected, freed of meninges, and diced into small fragments. Cortical fragments were incubated in 2.5% trypsin and 2 mg/ml DNase I in phosphate-buffered saline (PBS) (8.1 mM Na_2HPO_4, 1.5 mM KH_2PO_4, 137 mM NaCl, and 2.7 mM KCl; pH 7.4) at 37°C for 15 min. The fragments were then dissociated into single cells by pipetting. The dissociated cells were suspended in a feeding medium and plated onto poly-D-lysine-coated 12-well plates at a cell density of 1×10^6/ml in Dulbecco modified Eagle's medium nutrient mixture (DMEM/F-12; 50:50%) containing N_2 supplements plus 7.5% bovine albumin fraction V.

Highly astrocyte-rich cultures were prepared according to a previously described method (Michikawa et al., 2001). In brief, brains of postnatal day 2 ApoE knockout mice were removed under anesthesia. The cerebral cortices from the mouse brains were dissected, freed of meninges, and diced into small fragments. Cortical fragments were incubated in 0.25% trypsin and 2 mg/ml DNase I in PBS (8.1 mM Na_2HPO_4, 1.5 mM KH_2PO_4, 137 mM NaCl and 2.7 mM KCl; pH 7.4) at 37°C for 15 min. The fragments were then dissociated into single cells by pipetting. The dissociated cells were seeded in 75-cm^2 dishes at a cell density of 1×10^7 in DMEM nutrient mixture containing 10% FBS and 1% penicillin/streptomycin solution (Invitrogen Corporation, Carlsbad, CA). After 10 days of incubation in vitro, astrocytes in the monolayer were trypsinized (0.1%) and reseeded onto twelve-well dishes. The astrocyte-rich cultures were maintained in DMEM containing 10% FBS until use.

ApoE Preparation

The full-length human ApoE3 and ApoE4 and their 22- and 10-kDa fragments were expressed and purified as described (Saito et al., 2001). The cDNA for full-length human ApoE3 and ApoE4, the 22-kDa fragments, or the 10-kDa fragment were ligated into a thioredoxin fusion expression vector pET32a and transformed into the *Escherichia coli* strain BL21 star (DE3). The transformed *E. coli* were cultured in LB medium at 37°C, and thioredoxin-ApoE expression was induced with isopropyl-β-D-galactopyranoside for 3 hr. After the bacterial pellet was sonicated and the lysate was centrifuged to remove debris, the fusion protein was cleaved with thrombin to remove thioredoxin from full-length ApoE3, ApoE4 or the 22- or 10-kDa fragment. For the full-length ApoE3 and ApoE4, the fusion protein was complexed with DMPC before it was cleaved with thrombin to protect the protease susceptible internal hinge region. After inactivation of the thrombin with β-mercaptoethanol, the mixture was lyophilized and delipidated, and the ApoE pellet was dissolved in 6 M guanidine–HCl, pH 7.4, containing 1% β-mercaptoethanol. The ApoE was isolated by gel filtration chromatography on a Sephacryl S-300 column. For further purification (>95%), the proteins were subjected to gel filtration with a Superdex 75 column or anion exchange chromatography with a HiTrap Q column

When we used ApoE and ApoE fragments, the recombinant ApoEs were dissolved in 5 M guanidine–HCl. The resulting solutions were dialyzed against PBS at 4°C for 16 hr. Each ApoE level was determined with a BCA protein assay kit (Pierce, Rockford, IL).

Determination of Levels of Cholesterol and Phosphatidylcholine (PC) Released From Neurons and Astrocytes Labeled With [^{14}C]acetate

Astrocytes plated in twelve-well dishes were cultured in DMEM containing 10% FBS and 1% penicillin/streptomycin

solution for 72 hr. The cultures were then treated with 37 kBq/ml [^{14}C]acetate (Moravek Biochemicals Inc., Brea, CA) for 48 hr. The astrocytes were washed in DMEM two times and treated with 0.3 μM ApoE in DMEM for 24 hr. To analyze dose-dependent effects, the astrocytes were treated with 0.03 μM, 0.1 μM, 0.3 μM and 1.0 μM ApoE; to analyze time-dependent effects, the astrocytes were treated and maintained for 8, 24 and 48 hr. The culture medium was quickly removed and the astrocytes were dried at room temperature. 1.0 ml of the conditioned culture medium was extracted with 4.0 ml of hexane/isopropyl alcohol (3:2 v/v). For the extraction of intracellular lipids, dried astrocytes were incubated in hexane/isopropyl alcohol (3:2 v/v) for 1 hr at room temperature. The solvent from each plate was removed and dried under N_2 gas. The organic phase was redissolved in 200 μl of hexane/isopropyl alcohol (3:2 v/v), and 10 μl of each sample was spotted on activated-silica-gel high- performance thin layer chromatography plates (Merck); the lipids were separated by sequential one-dimensional chromatography by using chloroform/methanol/acetic acid/water (25:15:4:2, v/v), followed by another run in hexane/diethyl ether/acetic acid (80:30:1). [^{14}C]Cholesterol and [^{14}C]PC were used as standards. The chromatography plates were exposed to radiosensitive films, and each lipid was visualized and quantified with BAS2500 (Fuji Film, Tokyo, Japan). The levels of [^{14}C]cholesterol and [^{14}C]PC efflux were calculated by the following formula: % efflux = media × 100/(media + cell).

Dimerization of 22-kDa-ApoE3

The pure 22-kD-ApoE3 was obtained by reduction with 10 mM dithiothreitol (DTT) in 5 M guanidine–HCl buffer. The dimer was formed by incubation of the monomer in oxygenated 5 M guanidine–HCl at 10 mg/ml for 2 weeks at 4°C. Residual monomer was removed by passage of the protein solution through a thiopropyl Sepharose 6B column (GE Healthcare, Piscataway, NJ) according to the manufacturer's instructions.

Dimerization of Intact ApoE3

The ApoE3 (1 mg/ml in 6 M urea, and 10 mM Tris-HCl) used was a mixture of monomeric and dimeric ApoEs. The mixture was reduced to generate monomeric ApoE3 by adding 10 mM DTT, incubated at 4°C for 16 hr, dialyzed against 6 M urea in 10 mM Tris-HCl solution, and oxidized by stirring at 4°C for 3 days. Then it was loaded onto a 2-ml-bed-volume prepacked 6% cross-linked beaded agarose gel column with a SulfoLink kit (Pierce, Rockford, IL) and equilibrated with PBS. Dimeric ApoE3 was eluted with PBS.

Western Blot Analysis of Dimeric 22-kDa-ApoE3 by Nonreducing Gel Electrophoresis

To determine the ratio of dimeric 22-kDa-ApoE3 in the solution, Western blot analysis was performed under nonreducing conditions. Dimeric 22-kDa-ApoE3 was mixed with the same volume of a 2× nonreducing Laemmli buffer consisting of 100 mM Tris-HCl (pH 7.4), 10% glycerol, 4% SDS, and 0.01% bromophenol blue, and analyzed by 4–12% Tris/Tricine sodium dodecyl sulfate–polyacrylamide gel electrophoresis (SDS-PAGE) (Daiichi Pure Chemicals Co., Tokyo, Japan). The separated proteins were transferred onto Immobilon membranes with a semidry electrophoretic transfer apparatus (Nihon Eido, Tokyo, Japan) with a transfer buffer (0.1 M Tris-HCl (pH 7.4), 0.192 M glycine, and 20% methanol). The blots were probed for 16 hr at 4°C with a goat anti-ApoE polyclonal antibody, AB947 (1:2,000; Chemicon, Temecula, CA). Band detection was carried out with an ECL kit (GE Healthcare UK Ltd., England).

Purification and Carboxamidomethylation of Recombinant Intact ApoE3

ApoE3 was dissolved in 5 M guanidine–HCl, 10 mM EDTA, 200 mM Tris-HCl (pH8.5), and half of each protein solution was reduced with 10 mM DTT at room temperature for 2 hr and alkylated with 40 mM iodoacetamide in the dark at room temperature for 30 min, as described previously (Franceschini et al., 1990). All the proteins were then purified on an Aquapore RP300 column (2.1 × 30 mm; Applied Biosystems; Foster City, CA) by reverse-phase high-performance liquid chromatography (HPLC; model 1100 Series; Agilent Technology, Waldbronn, Germany) with a linear gradient of 36–52% acetonitrile in 0.1% trifluoroacetic acid for 16 min and a linear gradient of 52–76% acetonitrile in 0.1% trifluoroacetic acid for 1 min at a flow rate of 0.2 ml/min. The HPLC-purified ApoE3 was lyophilized and kept at −30°C until use.

Effect of 22-hydroxycholesterol and Glyburide on 22-kDa-ApoEs-induced Lipid Efflux

Neuron cultures were prepared, maintained, and labeled with [^{14}C]acetate, and exposed to 22-kDa-ApoE3 dimer or 22-kDa-ApoE3 monomer at a concentration of 0.3 μM in the presence of 22-hydroxycholesterol (10 μM) or glyburide (500 μM) for 24 hr. The lipids released into the media and the lipids retained in the cells were then determined. The expression level of ABCA1 in the cultures for each treatment was determined by Western blot analysis with anti-ABCA1 antibody (Santa Cruz, Santa Cruz, CA) used as a primary antibody.

RNA Interference

To knock down the endogenous ABCA1, primary cultured neurons and astrocytes were transiently transfected with 50 nM of the synthesized small interfering RNAs (siRNAs) targeting ABCA1 or with the Stealth siRNA negative control (Invitrogen) with Lipofectamine RNAiMAX (Invitrogen) according to the manufacturer's protocol. ABCA1 siRNA sequences is as follows: ABCA1-siRNA sense (5′-CA GGAUUUCCUGGUGGACAAUGAAA-3′) and antisense (5′-UUUCAUUGUCCACCAGGAAAUCCUG-3′).

Statistical Analysis

StatView computer software (Windows) was used for statistical analysis. The statistical significance of differences between samples was evaluated by multiple pairwise comparisons among the sets of data by ANOVA and the Bonferroni *t*-test.

RESULTS

Primary-cultured neurons and astrocytes were prepared and the levels of cholesterol and PC efflux were determined as described in Experimental Procedures. The levels of cholesterol and PC released from neurons in the medium treated with ApoE3 at 0.3 μM were significantly greater than those in the medium treated with ApoE4 (Fig. 1A). The level of cholesterol released by ApoE4 was 25% of that released by ApoE3. The reduced levels of cholesterol and PC efflux induced by ApoE4 increased significantly, although not to the level induced by ApoE3, when the neurons were incubated with the apoE4 (E255A) mutant (mt-ApoE4), which has altered amino- and carboxyl-terminal domain interaction because there is no electrostatic interaction between Arg61 and Glu255 (Dong and Weisgraber, 1996) (Fig. 1A). The partial recovery in the level of lipid efflux induced by mt-ApoE4 suggests that mechanisms other than the domain interaction are involved in ApoE-isoform-dependent lipid efflux from neurons in culture. Similar results were observed with cultured astrocytes. The levels of cholesterol and PC released from astrocytes in the medium treated with ApoE3 at 0.3 μM were significantly greater than those in the medium treated with ApoE4 (Fig. 1B). The levels of cholesterol and PC efflux induced by ApoE4 increased significantly, although not to the level induced by ApoE3, when the astrocytes were incubated with mt-ApoE4 (Fig. 1B).

We also examined the effect of the ApoE fragments on lipid efflux from cultured neurons and astrocytes to determine which part of the ApoE molecule is responsible for lipid efflux and ApoE isoform dependency. Interestingly, the 22-kDa fragment of ApoE (22-kDa-ApoE) induced cholesterol and PC efflux, which were ApoE-isoform-dependent (Fig. 1A,B). Unexpectedly, the carboxyl-terminal 10-kDa-ApoE and 12-kDa-ApoE, both of which contain the lipid binding site, have a very weak ability to release lipids (Fig. 1A,B).

Figure 2A shows the time-dependent cholesterol and PC efflux from neurons induced by 22-kDa-ApoE3 and 22-kDa-ApoE4 at 0.3 μM. The level of lipids released by 22-kDa-ApoE3 was significantly greater than that by 22-kDa-ApoE4 at time points of 24 and 48 hr (Fig. 2B). The level of cholesterol and PC efflux induced by 22-kDa-ApoE 24 hr after the treatment increased in an ApoE-concentration-dependent manner (Fig. 2B). The levels of cholesterol and PC efflux induced by 22-kDa-ApoE3 were greater than those released by 22-kDa-ApoE4 at 0.3 and 1.0 μM (Fig. 2B). Time- and ApoE-dose-dependent lipid efflux was also examined with ApoE-deficient astrocyte cultures, and the similar results were observed (Fig. 2C,D).

The results in Figures 1 and 2 indicate that the amino-terminal domain, the 22-kDa fragment, induces lipid efflux in an ApoE-isoform dependent manner, whereas the carboxyl-terminal domain, the 10-kDa fragment, has a very weak ability to induce lipid efflux from cultured astrocytes. These results raise the question of how the amino-terminal and carboxyl-terminal domains

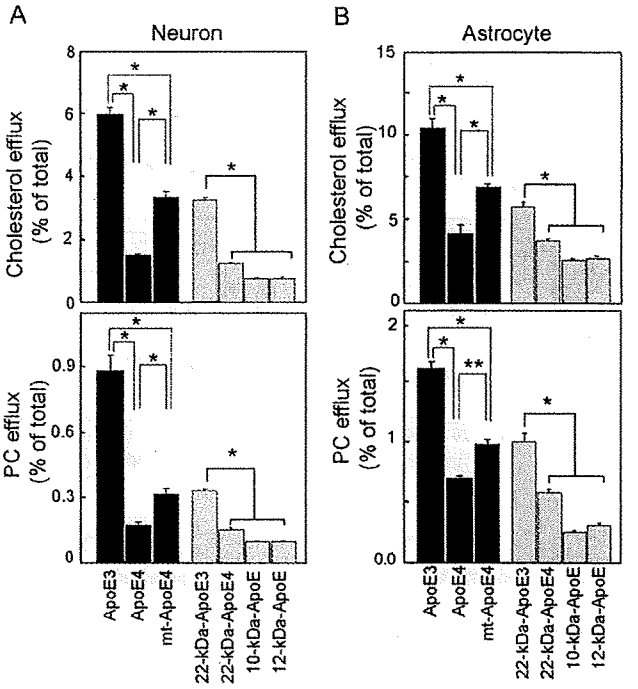

Fig. 1. Cholesterol and PC efflux from cultured neurons and astrocytes induced by ApoEs. Neurons and astrocytes were prepared as described in Experimental Procedures. The neurons (**A**) and astrocytes (**B**) were cultured for 72 hr, labeled with [^{14}C]acetate for 48 hr, and exposed to intact, lipid-free, ApoE3(residues 1–299), ApoE4, mt-ApoE4(E255A), 22-kDa-ApoE3 (residues 1–191), 22-kDa-ApoE4, 10-kDa-ApoE (residues 218–299), and 12-kDa-ApoE (residues 192–299) fragments at 0.3 μM for 24 hr. The lipids released into the media and the lipids retained in the cells were extracted and analyzed as described in Experimental Procedures. The percentages of released cholesterol and PC levels over the total levels were calculated. Data are means ± SE of four samples. $*P < 0.0001$ and $**P < 0.0005$. Three independent experiments showed similar results. The basal value of cholesterol and PC efflux in the absence of ApoEs are 1.0 ± 0.1 (%) and 0.4 ± 0.1 (%), respectively.

contribute to lipid efflux induced by intact ApoE in an ApoE-isoform-dependent manner. To answer this question, we examined whether the carboxyl-terminal domain of ApoE modifies lipid efflux caused by 22-kDa-ApoE. The ApoEs used were 22-kDa-ApoE (amino acids, 1–191) and 22-kDa-ApoE with carboxyl-terminal fragment of various lengths, that is, ApoEs harboring amino acids 1–250, 1–260, 1–272, and 1–299 (intact ApoE). As shown in Figure 3A, cholesterol and PC efflux induced by ApoE3 species from cultured neurons depended on the carboxyl-terminal fragment length; that is, ApoE3 variants with a longer carboxyl-terminal region induced progressively more lipid efflux. However, such is not the case for ApoE4. The addition of a carboxyl-terminal region ending at amino acid 250 increased the level of lipid efflux significantly more than 22-kDa-ApoE4; however, 22-kDa-ApoE4 with a car-

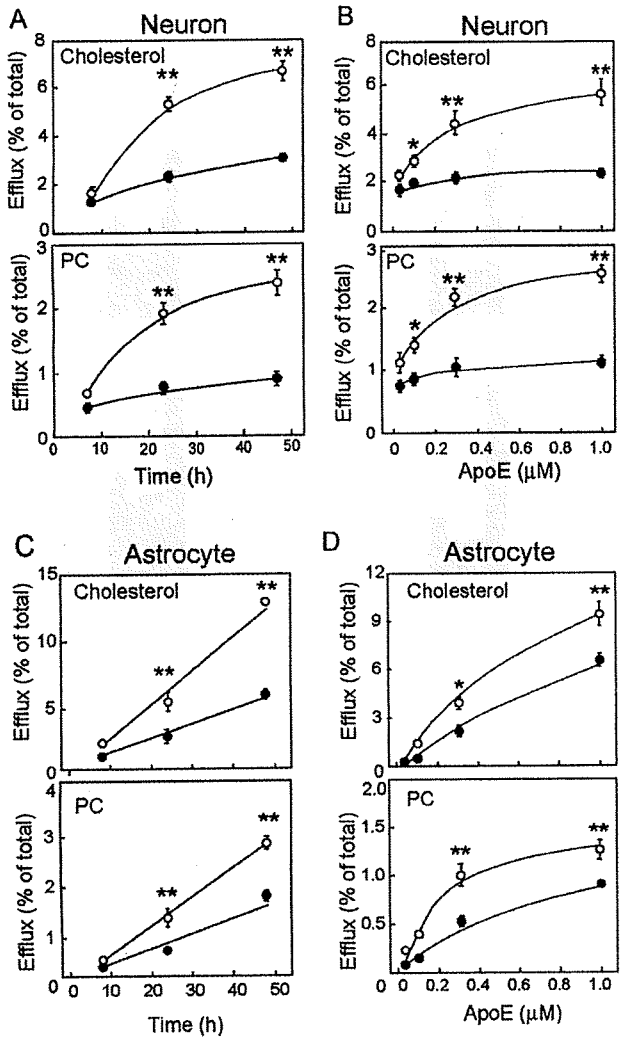

Fig. 2. Time- and dose-dependent lipid efflux mediated by 22-kDa-ApoE fragment. Cultured neurons and astrocytes were prepared, maintained, and labeled with [^{14}C]acetate as described in the legend for Fig. 1. For determination of the time-dependent lipid release from neurons (**A**) and astrocytes (**C**), each culture was exposed to 22-kDa-ApoE3 (open circle) and 22-kDa-ApoE4 (closed circle) at 0.3 μM for 8, 24, and 48 hr. For determination of the dose-dependent lipid release from neurons (**B**) and astrocytes (**D**), each culture was exposed to 22-kDa-ApoE3 (open circle) and 22-kDa-ApoE4 (closed circle) at varying concentrations for 24 hr. The lipids released into the media and the lipids retained in the cells were determined as described in Experimental Procedures. (**B**) For determination of Data are means ± SE of four samples. $*P < 0.05$ and $**P < 0.0005$ vs. 22-kDa-ApoE4 at each time point. The basal value of cholesterol and PC efflux in the absence of ApoEs are less than 0.8 ± 0.05 and 0.66 ± 0.11, respectively (**A**), and 0.59 ± 0.04 and 0.39 ± 0.04, respectively (**B**).

boxyl- terminal region longer than 250 amino acid residues lost the additional effect of the carboxyl-terminal region on lipid efflux. The levels of cholesterol and PC efflux induced by mt-ApoE4 recovered significantly but partially, and they did not reach those induced by intact ApoE3, similar to the result shown in Figure 1. Similar results were observed when ApoE-deficient astrocyte cultures were used (Fig. 3B).

The above results suggest that the amino-terminal domain basically determines the ability of ApoE to induce lipid efflux and that the carboxyl-terminal region enhances this ability when the amino and carboxyl domain interaction is absent. Because the absence or presence of cysteine at position 112 in the amino-terminal domain differentiates ApoE3 from ApoE4, it is possible to assume that this one-amino-acid difference results in intra- or intermolecular structural differences leading to the domain interaction or dimerization, respectively. Thus, we examined the effect of the dimer formation of 22-kDa-ApoE3 through disulfide bonds on lipid efflux from neurons and cultured astrocytes. To determine directly whether the dimeric form of 22-kDa-ApoE3 induces greater lipid efflux from astrocytes than the monomeric form, the pure dimeric form of 22-kDa-ApoE3 was prepared as described in Experimental Procedures. To obtain a solution containing the pure monomeric form of 22-kDa-ApoE3, 22-kDa-ApoE3 was dissolved in 5 M guanidine–HCl and 10 mM DTT. The resulting solutions were dialyzed against PBS at 4°C for 16 hr and used for the experiment. The purity of dimer and monomer in each sample was confirmed by Western blot analysis (Fig. 4). We also used 22-kDa-ApoE4 as monomeric ApoE molecule for the experiment that used astrocyte cultures because 22-kDa-ApoE4 contains no cysteine and it remains monomeric (Fig. 4B). The results demonstrated that dimeric form of 22-kDa-ApoE3 induced greater lipid efflux than the monomeric form of 22-kDa-ApoE3 and 22-kDa-ApoE4 in both neuron and astrocyte cultures (Fig. 4). Importantly, regardless of ApoE isoform, monomeric 22-kDa-ApoEs induces similar level of lipid efflux (Fig. 4B).

To determine whether such is the case for intact ApoEs, we examined the effect of the dimer formation of ApoE3 through disulfide bonds on lipid efflux from cultured neurons. We obtained dimer-enriched ApoE3 solutions by using a SulfoLink kit as described under Experimental Procedures. We also used ApoE3 solutions prepared without dimer enrichment, containing monomers and relatively few dimers. We also examined the effect of monomeric ApoEs, namely ApoE4 and ApoE3, whose cysteine was modified by carboxamidomethylation (ApoE3-CM). The levels of cholesterol and PC released from neurons treated with dimer-enriched ApoE3 were 2.9- and 7.6-fold greater than those released from neurons treated with ApoE3 and ApoE3 monomers (ApoE3-CM), respectively (Fig. 5). The effects of ApoE3-CM and ApoE4 on lipid efflux were similar. A Western blot analysis of each sample was performed and results show that the samples contained different amounts of dimers (Fig. 5B). The percentages of ApoE3 dimers as calculated by a densitometric analysis of the bands on the Western blot films were 64.5%,

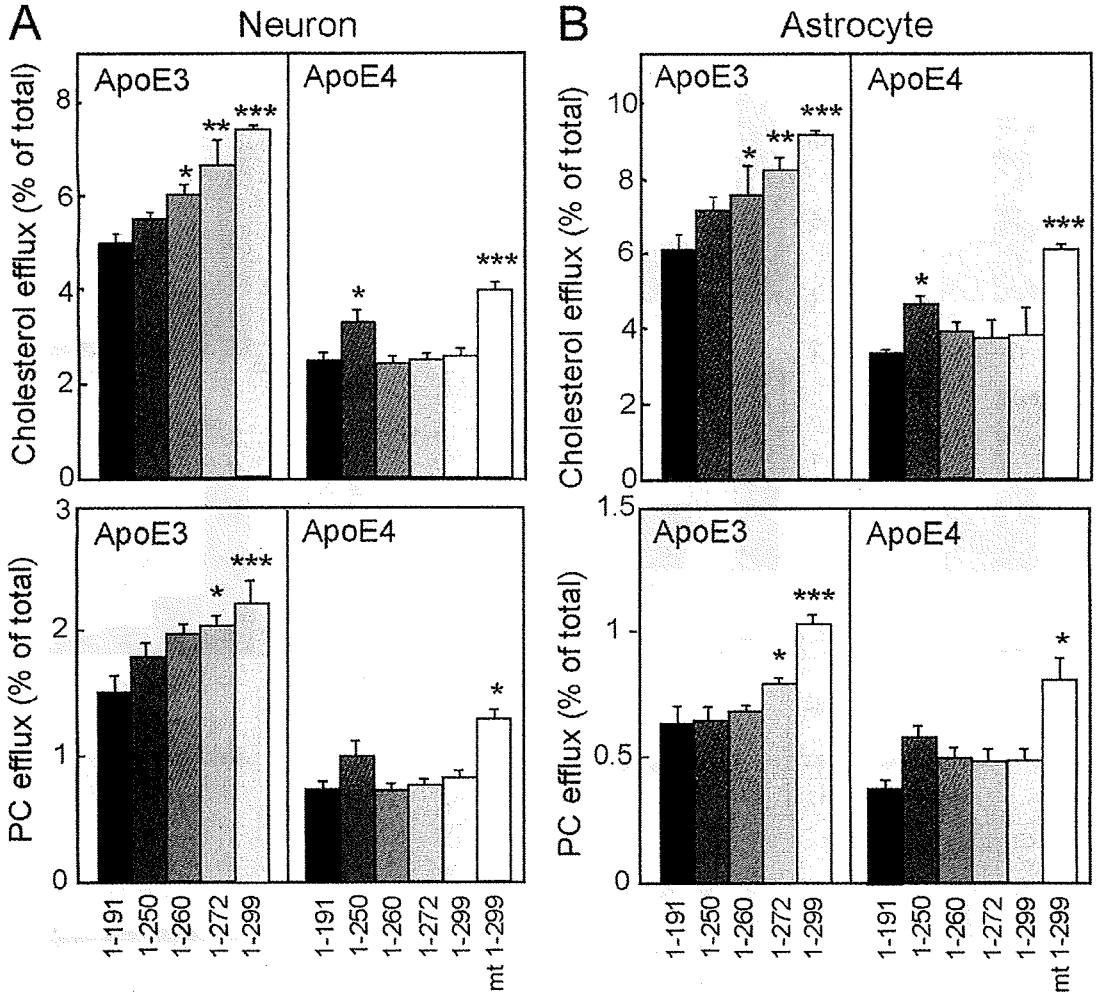

Fig. 3. Cooperative effects of amino- and carboxyl-terminal regions of ApoE on lipid efflux. Neurons and astrocytes were prepared, maintained, and labeled with [^{14}C]acetate as described in the legend for Fig. 1. The neurons (**A**) and astrocytes (**B**) were then exposed to ApoE with carboxyl-terminal regions of various lengths including 1–250, 1–260, 1–272, and 1–299 (full-length ApoE) at 0.3 μM for 24 hr, and the lipids released into the media and the lipids retained in the cells were determined as described in Experimental Procedures. For comparison, the effect of mt-ApoE4 was also determined. Data are means ± SE of four samples. $*P < 0.05$, $**P < 0.005$, and $***P < 0.0001$ vs. 22-kDa-ApoE (1–191). The basal value of cholesterol and PC efflux in the absence of ApoEs are less than 0.8 ± 0.05 and 0.66 ± 0.11, respectively (A, B).

36.9%, 1.8%, and 1.4% in the dimer-enriched ApoE3, non-dimer-enriched ApoE3, ApoE3-CM, and ApoE4 samples, respectively.

Next we determined the involvement of ABCA1 in 22-kDa-ApoEs-induced lipid efflux. The neuron cultures were treated with 22-kDa-ApoE3 dimers, 22-kDa-ApoE3 monomers, or 22-kDa-ApoE4 (monomers) concomitant with 10 μM of 22-hydroxycholesterol, an LXR ligand to up-regulate *ABCA1* gene expression (Wang et al., 2001), and the cultures were maintained for 24 hr. After 24 hr incubation, the level of lipids released into the medium was determined. The ABCA1 expression level was enhanced when the neurons were treated with 22-hydroxycholesterol (Fig. 6A). The levels of lipids released by these ApoE fragments were significantly enhanced when the cultures were concomitantly treated with 22-hydroxycholesterol (Fig. 6B). These results suggest that ABCA1 plays a key role in 22-kDa-ApoEs-mediated lipid efflux in neurons. In support of this notion, we have observed that the treatment of neurons with glyburide, an inhibitor of the ABCA1 transporter, resulted in decreased levels of 22-kDa-ApoE3-mediated cholesterol efflux (Fig. 6C). We further examined the effect of ABCA1 knockdown on 22-kDa ApoEs-mediated lipid efflux by using specific siRNAs. The knockdown of ABCA1 in neurons significantly reduced lipid efflux induced by 22-kDa-ApoE3 dimers (Fig. 7).

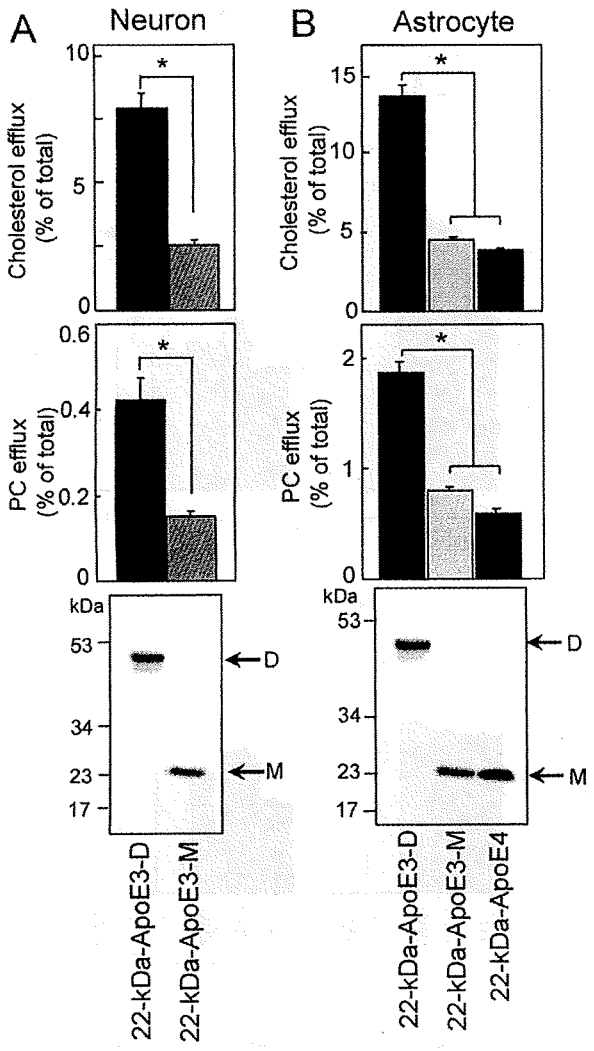

Fig. 4. The ability of 22-kDa-ApoE to induce lipid efflux depends on the ApoE self-association state, i. e., monomer vs dimer. Preparation of 22-kDa-ApoE3 dimer (22-kDa-ApoE3-D), monomer (22-kDa-ApoE3-M), or 22-kDa-ApoE4 monomer was performed as described in Experimental Procedures. **A:** The same amount of 22-kDa-ApoE3-D or 22-kDa-ApoE3-M was subjected to SDS-PAGE under nonreducing conditions, and Western blot analysis was performed with the anti-ApoE antibody AB947. D; dimers, M; monomer. Neuron cultures were prepared, maintained, and labeled with [^{14}C]acetate and exposed to 22-kDa-ApoE3-D or 22-kDa-ApoE3-M at 0.3 μM for 24 hr. The cholesterol and PC efflux by dimeric and monomeric 22-kDa-ApoE3 was determined. **B:** The same amount of 22-kDa-ApoE3 dimers, 22-kDa-ApoE3 monomers, and 22-kDa-ApoE4 monomers was subjected to SDS-PAGE under nonreducing conditions, and Western blot analysis was performed with the anti-ApoE antibody AB947. D; dimers, M; monomer. Astrocyte cultures were prepared, maintained, and labeled with [^{14}C]acetate and exposed to 22-kDa-ApoE3-D, 22-kDa-ApoE3-M, or 22-kDa-ApoE4 monomer at 0.3 μM for 24 hr. The cholesterol and PC efflux by dimeric and monomeric 22-kDa-ApoE3, and monomeric 22-kDa-ApoE4 was determined. Data are means ± SE of four samples. *$P < 0.0001$ vs. 22-kDa-ApoE3. The basal value of cholesterol and PC efflux in the absence of ApoEs are less than 1.41 ± 0.06 and 0.55 ± 0.03, respectively (A, B).

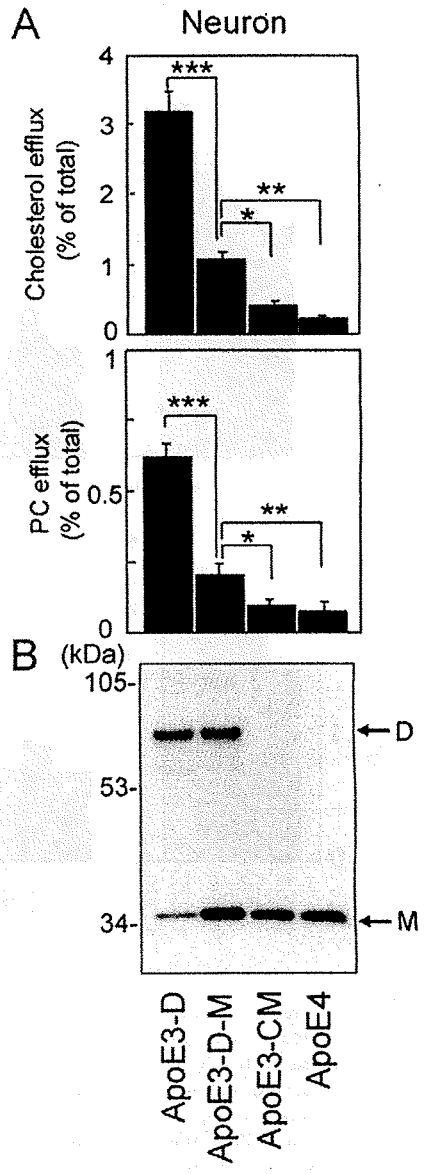

Fig. 5. Effect of intact ApoE dimers on lipid efflux from cultured neurons. A dimer-rich ApoE3 solution was obtained with a column that traps SH residues (monomeric ApoE3s). Carboxamidomethylated ApoE with iodoacetamide was prepared as described in Experimental Procedures. Neuronal cultures were prepared, maintained, and labeled with [^{14}C]acetate and exposed to dimer-enriched ApoE3, ApoE3, ApoE3-CM, and ApoE4 at 0.3 μM for 24 hr. **A:** The levels of cholesterol and PC released into the media and those retained in the cells were determined as described in Experimental Procedures. **B:** To determine the amount of dimers in the samples, Western blot analysis was performed under nonreducing conditions with anti-ApoE antibody AB947 used as the primary antibody. Data are means ± SE of four samples. *$P < 0.01$, **$P < 0.001$, ***$P < 0.0001$. The basal value of cholesterol and PC efflux in the absence of ApoEs are 1.54 ± 0.05 and 0.56 ± 0.05, respectively.

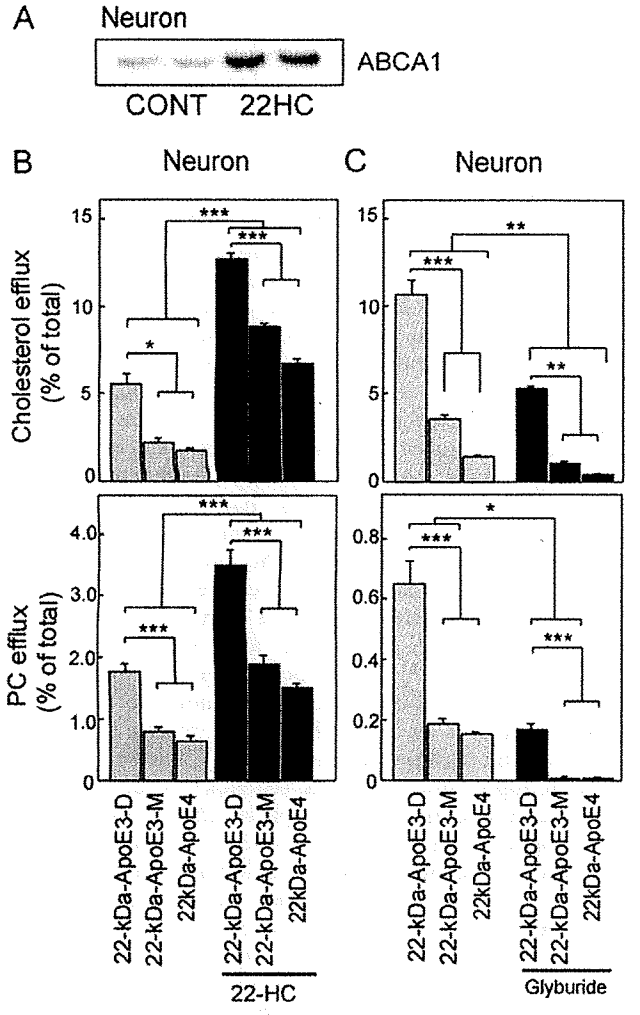

Fig. 6. The effect of 22-hydroxycholesterol and glyburide on 22-kDa-ApoEs-induced lipid efflux. Neuron cultures were prepared, maintained, and labeled with [^{14}C]acetate as described in Fig. 1, and exposed to 22-kDa-ApoE3 dimer (22-kDa-ApoE3-D), 22-kDa-ApoE3 monomer (22-kDa-ApoE3-M), or 22-kDa-ApoE4 at a concentration of 0.3 μM in the presence of 22-hydroxycholesterol (HC) at a concentration of 10 μM for 24 hr. (**A**) The expression level of ABCA1 in the cultures for each treatment was determined by Western blot analysis, and (**B**) the lipids released into the media and the lipids retained in the cells were determined. (**C**) [^{14}C]acetate-labeled neuron cultures were exposed to 22-kDa-ApoE3 dimer (22-kDa-ApoE3-D), 22-kDa-ApoE3 monomer (22-kDa-ApoE3-M), or 22-kDa-ApoE4 at a concentration of 0.3 μM in the presence of glyburide (500 μM) for 24 hr. The lipids released into the media and the lipids retained in the cells were determined. Data are means ± SE of four samples. $*P < 0.05$, $**P < 0.01$, and $***P < 0.0005$. Three independent experiments showed similar results. The basal value of cholesterol and PC efflux in the absence of ApoEs are 5.45 ± 0.51 and 0.58 ± 0.06, respectively.

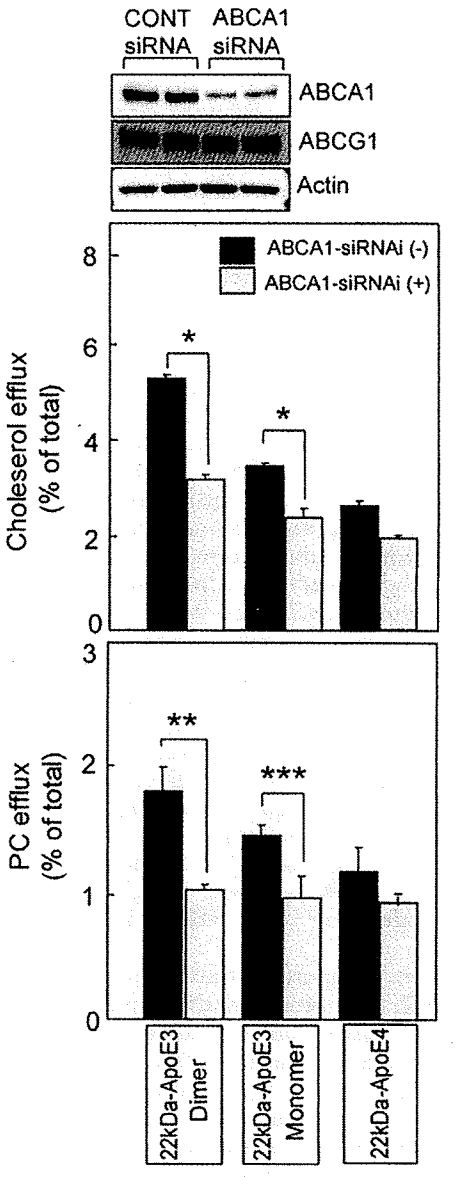

Fig. 7. Lipid efflux by 22-kDa-ApoEs is mediated by ABCA1. The primary neurons, which had been labeled with [^{14}C]acetate and treated with siRNA against ABCA1 for 48 hr, were exposed to 22-kDa-ApoE3 dimer (22-kDa-ApoE3-D) or 22-kDa-ApoE3 monomer (22-kDa-ApoE3-M) at a concentration of 0.3 μM, and maintained for 24 hr. The lipids released into the media and the lipids retained in the cells were then determined as described in Experimental Procedures. Data are means ± SE of four samples. $*P < 0.0001$, $**P < 0.002$, $***P < 0.02$. Three independent experiments showed similar results. The basal value of cholesterol and PC efflux in the absence of ApoEs are 0.89 ± 0.08 and 0.97 ± 0.14, respectively. Those values are 0.84 ± 0.08 and 0.46 ± 0.07 in the siABCA1 experiment.

DISCUSSION

We showed here that lipid efflux induced by ApoE is mainly mediated by the amino-terminal domain of ApoE and modified by the carboxyl-terminal domain. What we found are that the amino-terminal domain of ApoE induces lipid efflux in an isoform-dependent manner and the carboxyl-terminal domain enhances lipid efflux mediated by the amino-terminal domain of ApoE3. In contrast, the carboxyl-terminal domain does not strengthen the lipid efflux mediated by the amino-terminal domain of ApoE4 because of the domain interaction between the amino- and carboxyl-terminal domains. We also found that the lipid efflux induced by these ApoEs is mediated in an ABCA1-dependent manner.

Two of the main findings in this study are that the amino-terminal domain of ApoE, 22-kDa-ApoE, induces lipid efflux and that the extent of lipids released by the amino-terminal domain of ApoE, 22-kDa-ApoE3, is approximately 66% of that induced by intact ApoE3. The carboxyl-terminal domain synergistically and additively modifies lipid efflux mediated by 22-kDa-ApoE3. The additional contribution of the carboxyl-terminal domain is not observed in the case of ApoE4. Basically, 22-kDa-ApoE4 has a very weak ability to induce lipid efflux; moreover, the carboxyl-terminal region of ApoE does not effectively or additively enhance the lipid efflux mediated by 22-kDa-ApoE4. The lack of an additive effect by the carboxyl-terminal region on lipid efflux is likely due to the domain interaction, because an ApoE4 fragment ending at 250 (ApoE1–250) significantly gains in ability to release lipids; however, a carboxyl-terminal region longer than the amino acid 255, glutamate, which interacts with arginine at 61 (called the domain interaction; Dong and Weisgraber, 1996), does not induce any additive effect on lipid efflux induced by 22-kDa-ApoE4.

Another important finding regarding the effect of the domain interaction is that lipid efflux induced by mt-ApoE4 shows only a partial recovery toward the level exhibited by ApoE3. This indicates that the presence or absence of the amino and carboxyl domain interaction cannot completely explain ApoE-isoform-dependent lipid efflux mediated by intact ApoE and that other mechanisms are responsible for such ApoE-isoform dependency. This is supported by the finding of this study that 22-kDa-ApoE, which has no carboxyl-terminal region and thus has no domain interaction, induces lipid release in an ApoE-isoform-dependent manner.

We have already shown that α-helix formation is required for the high-affinity binding of apolipoprotein A-I to lipids (Saito et al., 2004), and that the binding capacity of 22-kDa-ApoE3 is lower than that of 22-kDa-ApoE4 for lipid particles (Saito et al., 2003). On the basis of the facts that the structural stabilities of 22-kDa-ApoE3 and 22-kDa-ApoE4 determine their binding affinity to lipids (Morrow et al., 2002; Segall et al., 2002; Weers et al., 2003) and that 22-kDa-ApoE4 is less stable than 22-kDa-ApoE3 (Morrow et al., 2000), it is reasonable to predict that the level of lipid efflux induced by 22-kDa-ApoE4 would be greater than that induced by 22-kDa-ApoE3. However, our results show the opposite, indicating that ApoE-isoform-dependent cholesterol efflux is unlikely to be explained by a simple theory linking the structural difference between these two fragments with their binding affinity to lipids.

Therefore, the question arises as to what is the mechanism underlying the isoform dependency of 22-kDa-ApoE-induced lipid efflux. It is possible to assume that 22-kDa-ApoE induces lipid efflux, because the 22-kDa domain contains an amphipathic four-helix bundle (Wilson et al., 1991), and it can bind to and reorganize phospholipid vesicles to form discoidal complexes (Lu et al., 2000; Segall et al., 2002). Surprisingly, 22-kDa-ApoE-induced lipid efflux is ApoE-isoform dependent. Such isoform dependency is likely to be caused by the presence or absence of cysteine at residue 112, which may result in intra- or intermolecular structural changes, forming dimers of 22-kDa-ApoE through disulfide bonds. More direct evidence that the dimeric form of 22-kDa-ApoE3 induces greater lipid efflux from cultured neurons and astrocytes than the monomeric form (Fig. 4) supports this idea. Previous reports have demonstrated that cellular cholesterol efflux is induced by many apolipoproteins in their lipid-free form, including ApoA-I, ApoA-II, ApoA-IV, and ApoCIII in addition to ApoE, all of which harbor multiple segments of amphiphilic helices (Segrest et al., 1992); the reaction still occurs with shorter apolipoproteins but to a lesser extent and only at high concentrations (Bielicki et al., 1992). Synthetic amphipathic helical peptides that mimic the physical properties of amphipathic helical segments of apolipoproteins can also induce cholesterol efflux as long as the peptide has at least two such helical segments (Mendez et al., 1994; Yancey et al., 1995). Consistent with these lines of evidence, when human ApoA-II, a disulfide-linked dimer, is reduced to a carboxyamidomethylation monomeric form, the ability of ApoA-II to induce cholesterol efflux is significantly decreased (Hara et al., 1992). In addition, the disulfide- linked homodimer of ApoE3 has been identified not only in cell culture medium (Gong et al., 2002), but also in human plasma (Weisgraber and Shinto, 1991). The mechanism by which the ApoE and ApoA-II dimers gain their functions to release higher amounts of lipids than ApoE and ApoA-II monomers, respectively, remains to be elucidated.

ABCA1 is involved in apolipoprotein-induced lipid efflux, including that mediated by ApoA-I (Brooks-Wilson et al., 1999; Lawn et al., 1999) and ApoE (Remaley et al., 2001; Krimbou et al., 2004). Regarding its effect on lipid efflux, the carboxyl-terminal fragment of ApoE (10-kDa-ApoE) induces a strong lipid efflux from non-CNS cells such as macrophages and ABCA1 plays a critical role in this efflux (Vedhachalam et al., 2007). Interestingly, contrary to these findings, 10-kDa-ApoE does not induce lipid efflux from the cultured neurons and astrocytes (Fig. 1). The reason for this discrepancy

remains unknown; however, the cell type difference may be a likely reason. In support of this notion, even intact ApoE3 induces a very low level of lipid efflux from macrophages or fibroblasts, and ABCA1 transfection induces a marked lipid efflux mediated by intact ApoE3 in these cells (Smith et al., 1996; Remaley et al., 2001). In contrast, intact ApoE3 itself induces marked lipid efflux from astrocytes without ABCA1 transfection as shown in this study. This may be because apolipoprotein-mediated cholesterol efflux is only apparent in growth-arrested cells (Mendez, 1997).

We have observed that pretreatment with 22-hydroxylcholesterol enhanced ABCA1 expression in neurons and cholesterol efflux induced by ApoE, suggesting that ABCA1 is involved in ApoE- and 22-kDa-ApoE3-mediated cholesterol efflux (Fig. 6). The involvement of ABCA1 has been also demonstrated by the fact that the knockdown of ABCA1 significantly reduced lipid efflux induced by 22-kDa ApoEs (Fig. 7). One cannot exclude the possibility that factors other than ABCA1 that are relevant to biological mechanisms are involved because the involvement of ATP-binding cassette protein G1 has been reported previously (Karten et al., 2006; Kim et al., 2007); however, the lines of evidence in our present study suggest that lipid efflux from cultured neurons induced by ApoE or an ApoE fragment is mediated by ABCA1 function.

It is reasonable to assume that the disruption of the ApoE4 domain interaction by, for example, small molecules that create the ApoE3-like structure is a potential therapeutic target in neurodegenerative diseases including AD (Mahley et al., 2006). However, if the role of ApoE in HDL generation and its supply to neurons are critically involved in neurodegeneration in AD, other approaches that do not modulate the acceptor function, but modulate the cellular factors including ABCA1 expression and subsequent HDL generation, could also be candidate therapeutic targets.

REFERENCES

Bielicki JK, Johnson WJ, Weinberg RB, Glick JM, Rothblat GH. 1992. Efflux of lipid from fibroblasts to apolipoproteins: dependence on elevated levels of cellular unesterified cholesterol. J Lipid Res 33:1699–1709.

Borghini I, Barja F, Pometta D, James RW. 1995. Characterization of subpopulations of lipoprotein particles isolated from human cerebrospinal fluid. Biochim Biophys Acta 1255:192–200.

Boyles JK, Pitas RE, Wilson E, Mahley RW, Taylor JM. 1985. Apolipoprotein E associated with astrocytic glia of the central nervous system and with nonmyelinating glia of the peripheral nervous system. J Clin Invest 76:1501–1513.

Brooks-Wilson A, Marcil M, Clee SM, Zhang LH, Roomp K, van Dam M, Yu L, Brewer C, Collins JA, Molhuizen HO, Loubser O, Ouelette BF, Fichter K, Ashbourne-Excoffon KJ, Sensen CW, Scherer S, Mott S, Denis M, Martindale D, Frohlich J, Morgan K, Koop B, Pimstone S, Kastelein JJ, Hayden MR. 1999. Mutations in ABC1 in Tangier disease and familial high-density lipoprotein deficiency. Nat Genet 22: 336–345.

Corder EH, Saunders AM, Strittmatter WJ, Schmechel DE, Gaskell PC, Small GW, Roses AD, Haines JL, Pericak-Vance MA. 1993. Gene dose of apolipoprotein E type 4 allele and the risk of Alzheimer's disease in late onset families [see comments]. Science 261:921–923.

Demeester N, Castro G, Desrumaux C, De Geitere C, Fruchart JC, Santens P, Mulleners E, Engelborghs S, De Deyn PP, Vandekerckhove J, Rosseneu M, Labeur C. 2000. Characterization and functional studies of lipoproteins, lipid transfer proteins, and lecithin:cholesterol acyltransferase in CSF of normal individuals and patients with Alzheimer's disease. J Lipid Res 41:963–974.

Dong LM, Weisgraber KH. 1996. Human apolipoprotein E4 domain interaction. Arginine 61 and glutamic acid 255 interact to direct the preference for very low density lipoproteins. J Biol Chem 271:19053–19057.

Franceschini G, Calabresi L, Tosi C, Gianfranceschi G, Sirtori CR, Nichols AV. 1990. Apolipoprotein AIMilano. Disulfide-linked dimers increase high density lipoprotein stability and hinder particle interconversion in carrier plasma. J Biol Chem 265:12224–12231.

Gong JS, Kobayashi M, Hayashi H, Zou K, Sawamura N, Fujita SC, Yanagisawa K, Michikawa M. 2002. Apolipoprotein E (ApoE) isoform-dependent lipid release from astrocytes prepared from human ApoE3 and ApoE4 knock-in mice. J Biol Chem 277:29919–29926.

Hara H, Komaba A, Yokoyama S. 1992. Alpha-helical requirements for free apolipoproteins to generate HDL and to induce cellular lipid efflux. Lipids 27:302–304.

Hatters DM, Budamagunta MS, Voss JC, Weisgraber KH. 2005. Modulation of apolipoprotein E structure by domain interaction: differences in lipid-bound and lipid-free forms. J Biol Chem 280:34288–34295.

Karten B, Campenot RB, Vance DE, Vance JE. 2006. Expression of ABCG1, but not ABCA1, correlates with cholesterol release by cerebellar astroglia. J Biol Chem 281:4049–4057.

Kim WS, Rahmanto AS, Kamili A, Rye KA, Guillemin GJ, Gelissen IC, Jessup W, Hill AF, Garner B. 2007. Role of ABCG1 and ABCA1 in regulation of neuronal cholesterol efflux to apolipoprotein E discs and suppression of amyloid-beta peptide generation. J Biol Chem 282:2851–2861.

Krimbou L, Denis M, Haidar B, Carrier M, Marcil M, Genest J Jr. 2004. Molecular interactions between apolipoprotein E and the ATP-binding cassette transporter A1 (ABCA1): impact on ApoE lipidation. J Lipid Res 46:1457–1465.

LaDu MJ, Gilligan SM, Lukens JR, Cabana VG, Reardon CA, Van Eldik LJ, Holtzman DM. 1998. Nascent astrocyte particles differ from lipoproteins in CSF. J Neurochem 70:2070–2081.

Lawn RM, Wade DP, Garvin MR, Wang X, Schwartz K, Porter JG, Seilhamer JJ, Vaughan AM, Oram JF. 1999. The Tangier disease gene product ABC1 controls the cellular apolipoprotein-mediated lipid removal pathway. J Clin Invest 104:R25–31.

Lu B, Morrow JA, Weisgraber KH. 2000. Conformational reorganization of the four-helix bundle of human apolipoprotein E in binding to phospholipid. J Biol Chem 275:20775–20781.

Mahley RW, Weisgraber KH, Huang Y. 2006. Apolipoprotein E4: a causative factor and therapeutic target in neuropathology, including Alzheimer's disease. Proc Natl Acad Sci U S A 103:5644–5651.

Mendez AJ. 1997. Cholesterol efflux mediated by apolipoproteins is an active cellular process distinct from efflux mediated by passive diffusion. J Lipid Res 38:1807–1821.

Mendez AJ, Anantharamaiah GM, Segrest JP, Oram JF. 1994. Synthetic amphipathic helical peptides that mimic apolipoprotein A-I in clearing cellular cholesterol. J Clin Invest 94:1698–1705.

Michikawa M, Fan QW, Isobe I, Yanagisawa K. 2000. Apolipoprotein E exhibits isoform-specific promotion of lipid efflux from astrocytes and neurons in culture. J Neurochem 74:1008–1016.

Michikawa M, Gong JS, Fan QW, Sawamura N, Yanagisawa K. 2001. A novel action of Alzheimer's amyloid b-protein (Ab): oligomeric Ab promotes lipid release. J Neurosci 21:7226–7235.

Molander-Melin M, Blennow K, Bogdanovic N, Dellheden B, Mansson JE, Fredman P. 2005. Structural membrane alterations in Alzheimer brains found to be associated with regional disease development: increased density of gangliosides GM1 and GM2 and loss of cholesterol in detergent-resistant membrane domains. J Neurochem 92:171–182.

Morrow JA, Segall ML, Lund-Katz S, Phillips MC, Knapp M, Rupp B, Weisgraber KH. 2000. Differences in stability among the human apolipoprotein E isoforms determined by the amino-terminal domain. Biochemistry 39:11657–11666.

Morrow JA, Hatters DM, Lu B, Hochtl P, Oberg KA, Rupp B, Weisgraber KH. 2002. Apolipoprotein E4 forms a molten globule. A potential basis for its association with disease. J Biol Chem 277:50380–50385.

Nakai M, Kawamata T, Taniguchi T, Maeda K, Tanaka C. 1996. Expression of apolipoprotein E mRNA in rat microglia. Neurosci Lett 211:41–44.

Pitas RE, Boyles JK, Lee SH, Foss D, Mahley RW. 1987a. Astrocytes synthesize apolipoprotein E and metabolize apolipoprotein E–containing lipoproteins. Biochim Biophys Acta 917:148–161.

Pitas RE, Boyles JK, Lee SH, Hui D, Weisgraber KH. 1987b. Lipoproteins and their receptors in the central nervous system. Characterization of the lipoproteins in cerebrospinal fluid and identification of apolipoprotein B,E(LDL) receptors in the brain. J Biol Chem 262:14352–14360.

Raffai RL, Dong LM, Farese RV Jr, Weisgraber KH. 2001. Introduction of human apolipoprotein E4 "domain interaction" into mouse apolipoprotein E. Proc Natl Acad Sci U S A 98:11587–11591.

Ramaswamy G, Xu Q, Huang Y, Weisgraber KH. 2005. Effect of domain interaction on apolipoprotein E levels in mouse brain. J Neurosci 25:10658–10663.

Remaley AT, Stonik JA, Demosky SJ, Neufeld EB, Bocharov AV, Vishnyakova TG, Eggerman TL, Patterson AP, Duverger NJ, Santamarina-Fojo S, Brewer HB Jr. 2001. Apolipoprotein specificity for lipid efflux by the human ABCAI transporter. Biochem Biophys Res Commun 280:818–823.

Roheim PS, Carey M, Forte T, Vega GL. 1979. Apolipoproteins in human cerebrospinal fluid. Proc Natl Acad Sci U S A 76:4646–4649.

Saito H, Dhanasekaran P, Baldwin F, Weisgraber KH, Lund-Katz S, Phillips MC. 2001. Lipid binding-induced conformational change in human apolipoprotein E. Evidence for two lipid-bound states on spherical particles. J Biol Chem 276:40949–40954.

Saito H, Dhanasekaran P, Baldwin F, Weisgraber KH, Phillips MC, Lund-Katz S. 2003. Effects of polymorphism on the lipid interaction of human apolipoprotein E. J Biol Chem 278:40723–40729.

Saito H, Dhanasekaran P, Nguyen D, Deridder E, Holvoet P, Lund-Katz S, Phillips MC. 2004. Alpha-helix formation is required for high affinity binding of human apolipoprotein A-I to lipids. J Biol Chem 279:20974–20981.

Segall ML, Dhanasekaran P, Baldwin F, Anantharamaiah GM, Weisgraber KH, Phillips MC, Lund-Katz S. 2002. Influence of apoE domain structure and polymorphism on the kinetics of phospholipid vesicle solubilization. J Lipid Res 43:1688–1700.

Segrest JP, Jones MK, De Loof H, Brouillette CG, Venkatachalapathi YV, Anantharamaiah GM. 1992. The amphipathic helix in the exchangeable apolipoproteins: a review of secondary structure and function. J Lipid Res 33:141–166.

Smith JD, Miyata M, Ginsberg M, Grigaux C, Shmookler E, Plump AS. 1996. Cyclic AMP induces apolipoprotein E binding activity and promotes cholesterol efflux from a macrophage cell line to apolipoprotein acceptors. J Biol Chem 271:30647–30655.

Strittmatter WJ, Saunders AM, Schmechel D, Pericak-Vance M, Enghild J, Salvesen GS, Roses AD. 1993. Apolipoprotein E: high-avidity binding to beta-amyloid and increased frequency of type 4 allele in late-onset familial Alzheimer disease. Proc Natl Acad Sci U S A 90:1977–1981.

Vedhachalam C, Narayanaswami V, Neto N, Forte TM, Phillips MC, Lund-Katz S, Bielicki JK. 2007. The C-terminal lipid-binding domain of apolipoprotein E is a highly efficient mediator of ABCA1-dependent cholesterol efflux that promotes the assembly of high-density lipoproteins. Biochemistry 46:2583–2593.

Wang N, Silver DL, Thiele C, Tall AR. 2001. ATP-binding cassette transporter A1 (ABCA1) functions as a cholesterol efflux regulatory protein. J Biol Chem 276:23742–23747.

Weers PM, Narayanaswami V, Choy N, Luty R, Hicks L, Kay CM, Ryan RO. 2003. Lipid binding ability of human apolipoprotein E N-terminal domain isoforms: correlation with protein stability? Biophys Chem 100:481–492.

Weisgraber KH. 1990. Apolipoprotein E distribution among human plasma lipoproteins: role of the cysteine–arginine interchange at residue 112. J Lipid Res 31:1503–1511.

Weisgraber KH, Shinto LH. 1991. Identification of the disulfide-linked homodimer of apolipoprotein E3 in plasma. Impact on receptor binding activity. J Biol Chem 266:12029–12034.

Weisgraber KH, Roses AD, Strittmatter WJ. 1994. The role of apolipoprotein E in the nervous system. Curr Opin Lipidol 5:110–116.

Wetterau JR, Aggerbeck LP, Rall SC Jr, Weisgraber KH. 1988. Human apolipoprotein E3 in aqueous solution. I. Evidence for two structural domains. J Biol Chem 263:6240–6248.

Wilson C, Wardell MR, Weisgraber KH, Mahley RW, Agard DA. 1991. Three-dimensional structure of the LDL receptor-binding domain of human apolipoprotein E. Science 252:1817–1822.

Xu Q, Brecht WJ, Weisgraber KH, Mahley RW, Huang Y. 2004. Apolipoprotein E4 domain interaction occurs in living neuronal cells as determined by fluorescence resonance energy transfer. J Biol Chem 279:25511–15516.

Yancey PG, Bielicki JK, Johnson WJ, Lund-Katz S, Palgunachari MN, Anantharamaiah GM, Segrest JP, Phillips MC, Rothblat GH. 1995. Efflux of cellular cholesterol and phospholipid to lipid-free apolipoproteins and class A amphipathic peptides. Biochemistry 34:7955–7965.

The American Journal of Pathology, Vol. 175, No. 5, November 2009

DOI: 10.2353/ajpath.2009.090418

Neurobiology

Microglia Activated with the Toll-Like Receptor 9 Ligand CpG Attenuate Oligomeric Amyloid β Neurotoxicity in *in Vitro* and *in Vivo* Models of Alzheimer's Disease

Yukiko Doi,* Tetsuya Mizuno,* Yuki Maki,* Shijie Jin,* Hiroyuki Mizoguchi,† Masayoshi Ikeyama,‡ Minoru Doi,‡ Makoto Michikawa,§ Hideyuki Takeuchi,* and Akio Suzumura*

From the Department of Neuroimmunology and the Futuristic Environmental Simulation Center,† Research Institute of Environmental Medicine, Nagoya University, Nagoya; the Department of Materials Science and Engineering,‡ Nagoya Institute of Technology, Nagoya; and the Department of Alzheimer's Disease Research,§ National Institute for Longevity Sciences, National Center for Geriatrics and Gerontology, Aichi, Japan*

Soluble oligomeric amyloid β (oAβ) 1-42 causes synaptic dysfunction and neuronal injury in Alzheimer's disease (AD). Although accumulation of microglia around senile plaques is a hallmark of AD pathology, the role of microglia in oAβ1-42 neurotoxicity is not fully understood. Here, we showed that oAβ but not fibrillar Aβ was neurotoxic, and microglia activated with unmethylated DNA CpG motif (CpG), a ligand for Toll-like receptor 9, attenuated oAβ1-42 neurotoxicity in primary neuron-microglia co-cultures. CpG enhanced microglial clearance of oAβ1-42 and induced higher levels of the antioxidant enzyme heme oxygenase-1 in microglia without producing neurotoxic molecules such as nitric oxide and glutamate. Among subclasses of CpGs, class B and class C activated microglia to promote neuroprotection. Moreover, intracerebroventricular administration of CpG ameliorated both the cognitive impairments induced by oAβ1-42 and the impairment of associative learning in Tg2576 mouse model of AD. We propose that CpG may be an effective therapeutic strategy for limiting oAβ1-42 neurotoxicity in AD. *(Am J Pathol 2009, 175:2121–2132; DOI: 10.2353/ajpath.2009.090418)*

The senile plaque is a pathological hallmark of Alzheimer's disease (AD). Fibrillar amyloid β (fAβ), a major component of senile plaques, induces tau hyperphosphorylation and neuronal dystrophy.[1,2] Soluble oligomeric Aβ (oAβ) has been reported to exhibit higher neurotoxicity than fAβ. Naturally secreted oAβ inhibits hippocampal long-term potentiation and disrupts synaptic plasticity in rats *in vivo*[3]. In addition, oAβ induces neuronal reactive oxygen species (ROS) through a mechanism requiring *N*-methyl-D-aspartate receptor activation.[4] Exposure to oAβ induces rapid and massive neuronal death, while fAβ is required at higher concentrations and for longer incubations to cause neuronal dystrophy.[5]

Microglia, macrophage-like cells in the central nervous system, cluster both in and around senile plaques and have been proposed to have pivotal roles in the pathogenesis of AD. Microglia activated with Aβ may be involved in the inflammatory component of AD.[6] Both fAβ and oAβ stimulate microglial secretion of proinflammatory cytokines, chemokines, complement components, and free radicals.[7] However, microglia also perform neu-

Supported in part by a grant-in-aid for scientific research (grant C), Global Centers of Excellence program "Integrated Functional Molecular Medicine for Neuronal and Neoplastic Disorders" funded by Ministry of Education, Culture, Sports, Science, and Technology of Japan, the Program for Promotion of Fundamental Studies in Health Sciences of the National Institute of Biomedical Innovation, the Hori Information Science Promotion Foundation, a grant-in-aid for Scientific Research on Priority Areas-Research on Pathomechanisms of Brain Disorders-from the Ministry of Education, Culture, Sports, Science, and Technology of Japan, and a grant from the Ministry of Health, Labor and Welfare of Japan (Comprehensive Research on Aging and Health grant H20-007).

Y.D. and T.M. contributed equally to this paper.

Accepted for publication July 30, 2009.

Supplemental material for this article can be found on *http://ajp.amjpathol.org*.

Address reprint requests to Tetsuya Mizuno, Department of Neuroimmunology, Research Institute of Environmental Medicine, Nagoya University, Furo-cho, Chikusa-ku, Nagoya 464-8601, Japan. E-mail: tmizuno@riem.nagoya-u.ac.jp.

roprotective functions such as releasing neurotrophic factors[8] and phagocytosing and degrading Aβ.[9,10]

Toll-like receptor (TLR) ligands enhance microglial phagocytosis of Aβ. Peptidoglycan, a TLR2 ligand, and unmethylated DNA CpG motifs (CpG), a TLR9 ligand, increase Aβ phagocytosis through the G protein-coupled formyl peptide receptor-like 2.[11,12] Similarly, the TLR4 ligand lipopolysaccharide increases phagocytosis through the CD14 receptor.[13] However, microglia activated with TLR ligands also produce neurotoxic molecules such as proinflammatory cytokines, nitric oxide (NO), ROS, and peroxynitrite.[14] In particular, lipopolysaccharide-activated microglia produce a large amount of glutamate, a neurotransmitter but also potent neurotoxin.[15] Thus, factors that increase microglial clearance of oAβ without producing inflammatory mediators are candidates for the treatment of AD.

Here, we investigated the role of microglia in neurotoxicity mediated by oAβ1-42. We found that microglia activated with a low dose of CpG attenuated the neurotoxic effects of oAβ1-42 without producing other neurotoxic molecules *in vitro*. Moreover, intracerebroventricular (ICV) administration of CpG ameliorated the cognitive impairment induced by ICV injection of oAβ1-42 and the impairment of associative learning in Tg2576 mouse model of AD.

Materials and Methods

Cell Culture

The protocols for animal experiments were approved by the Animal Experiment Committee of Nagoya University. Primary neuronal cultures were prepared from the cortices of embryonic day 17 (E17) C57BL/6 mice embryos as described previously.[8] Briefly, cortical fragments were dissociated into single cells in dissociation solution (Sumitomo Bakelite, Akita, Japan) and resuspended in Nerve Culture Medium (Sumitomo Bakelite). Neurons were plated onto 12-mm-polyethyleneimine-coated glass coverslips (Asahi Techno Glass, Chiba, Japan) at a density of 5×10^4 cells/well in 24-well multidishes and incubated at 37°C in a humidified atmosphere containing 5% CO_2. The purity of the cultures was >95% as determined by NeuN-specific immunostaining. Microglia were isolated on 14 days *in vitro* with the "shaking off" method previously described from primary mixed glial cell cultures prepared from newborn C57BL/6 mice.[16] Cultures were 97 to 100% pure as determined by Fc receptor-specific immunostaining and were maintained in Dulbecco's modified Eagle medium supplemented with 10% fetal calf serum, 5 μg/ml bovine insulin, and 0.2% glucose. Microglia were plated at a density of 7×10^4 cells/well in 8-well glass slides or at a density of 7×10^4 cells/well in 48-well multidishes. Neuron-microglia co-cultures were prepared as follows: 1×10^5 microglia in 100 μl of neuronal medium were added to neuronal cultures (5×10^4 neuronal cells) on 13 day *in vitro* in 24-well multidishes.

Preparations of Aβ Solutions

fAβ1-42 was prepared as described previously.[17] Briefly, synthetic human Aβ1-42 (Peptide Institute, Osaka, Japan) was dissolved in 0.02% ammonia solution at a concentration of 250 μmol/L, diluted to 25 μmol/L in PBS, and incubated at 37°C for 24 hours. oAβ1-42 was prepared as described previously.[18] Briefly, Aβ1-42 was dissolved to 1 mmol/L in 100% 1,1,1,3,3,3-hexafluoro-2-propanol. 1,1,1,3,3,3-Hexafluoro-2-propanol was dried by the vacuum desiccator and resuspended to 5 mmol/L in DMSO. To form oligomers, amyloid peptide was diluted to a final concentration of 100 μmol/L with Ham's F-12 and incubated at 4°C for 24 hours and then immediately added to cultures at a final concentration 5 μmol/L.

Transmission Electron Microscopy

To assess quaternary structures of Aβ, oAβ1-42 and fAβ1-42 solutions were spread on carbon-coated grids. Negative staining was performed with 3% phosphotungstic acid (pH 7.0). Proteins were then examined with a JEM-2000ExII Electron Microscope with an acceleration voltage of 160 kV.

Thioflavin T Assay

Optimum fluorescence measurements of amyloid fibrils were obtained at excitation and emission wavelength of 446 and 490 nm, respectively, with a reaction mixture containing 5 μmol/L thioflavin T (Nakalai tesque, Kyoto, Japan) and 50 mmol/L glycine-NaOH buffer (pH 8.5). Ten microliters of oAβ1-42 or fAβ1-42 solution was mixed with 100 μl of the reaction mixture, respectively.

Measurement of Heme Oxygenase-1, Interleukin-10, Matrix Metalloproteinase-9, Tumor Necrosis Factor-α, NO, and Glutamate

To measure factors produced by microglia treated with CpG and oAβ1-42, microglia were plated at a density of 7×10^4 cells/well (300 μl) in 48-well multidishes and then treated with 100 nmol/L CpG-DNA (HyCult Biotechnology, Uden, Netherlands), 100 nmol/L class A CpG (synthetic oligodeoxynucleotides (ODNs) 1585), class B CpG (ODN 1668), and class C CpG (ODN 2395). These CpG subtypes were from Alexis Biochemicals (San Diego, CA). After 3 hours of treatment with CpG, 5 μmol/L oAβ1-42 was added for 24 hours. Supernatants from microglia were assessed by ELISA kits for tumor necrosis factor-α (TNF-α) and interleukin (IL)-10 (BD Pharmingen, Franklin Lakes, NJ) and matrix metalloproteinase (MMP)-9 (R&D Systems, Minneapolis, MN). Cell extracts from microglia in extraction buffer (1% Nonidet P-40 in PBS) were measured for heme oxygenase-1 (HO-1) with an ELISA kit (Takara Bio, Mie, Japan). Measurement of NO was determined using the Griess reaction.[19] To measure glutamate, Glutamate Assay Kit colorimetric assay (Yamasa, Tokyo, Japan) was used as described previously.[20]

The mRNA expression of HO-1 was assessed by RT-PCR. Briefly, total RNA was extracted using the guanidinium thiocyanate method (RNeasy Mini Kit; Qiagen, Valencia, CA). cDNAs were generated by RT-PCR using SuperScript II (Invitrogen, Carlsbad, CA) and Ampli TaqDNA polymerase (Applied Biosystems, Branchburg, NJ) in the presence of the specific primers. HO-1 sense, 5′-CTATGTAAAGCGTCTCCA-3′; and HO-1 antisense, 5′-GTCTTTGTGTTCCTCTGTC-3′.

Measurement of ROS

To measure ROS in neuron-microglia co-cultures, we used the acetate ester form of 2′,7′-dichlorofluorescein diacetate (H_2DCFDA-AM) probe (Invitrogen). After neuron-microglia co-cultures were treated with or without 100 nmol/L CpG for 3 hours, cells were loaded with dye by replacing media with fresh nerve culture medium containing 5 μmol/L H_2DCFDA-AM for 30 minutes. After washing, culture medium containing 5 μmol/L oAβ1-42 was added and the fluorescence of the wells was measured. Fluorescent measurements were made using a Wallac 1420 ARVOMX (PerkinElmer Japan, Yokohama, Japan).

Immunocytochemistry

Neuronal, microglial, and neuron-microglia co-cultures were fixed with 4% paraformaldehyde for 30 minutes at room temperature, then blocked with 5% normal goat serum in PBS and permeabilized with 0.3% Triton X-100. Neurons were stained with rabbit polyclonal anti-microtubule-associated protein (MAP)-2 antibody (1/500; Chemicon, Temecula, CA) and secondary antibodies conjugated to Alexa 488 (1/1000; Invitrogen). Synthetic Aβ was stained with a mouse monoclonal anti-Aβ antibody (4G8) (1/1000; Chemicon) and secondary antibodies conjugated to Alexa 568 or 647. Microglia were stained with phycoerythrin-conjugated rat anti-mouse CD11b monoclonal antibody (1/300; BD Pharmingen) before fixation. Images were analyzed with a deconvolution fluorescent microscope system (BZ-8000; Keyence, Osaka, Japan). To assess neuronal death induced by Aβ, purified neurons (5×10^4 cells/well) were plated in 24-well multidishes. A total of 5 μM oAβ1-42 or fAβ1-42 was added to the cultures on 13 days *in vitro* for 24 hours. To assess neuronal death in neuron-microglia co-cultures, 3 hours after treatment with or without TLR ligands, 5 μmol/L oAβ1-42 was added to cultures for 24 hours. Surviving neurons were identified by cytoskeletal morphology of neurons as described previously.[8] Viable neurons stained strongly with an anti-MAP-2 antibody, whereas damaged neurons stained more weakly. The number of MAP-2-positive neurons was counted in representative areas per well. More than 200 neurons were examined in each of five independent trials by a scorer blind to the experimental condition. The number of untreated viable neurons was normalized to 100%.

Western Blotting

Neuronal cultures were treated with 5 μmol/L oAβ1-42 for 24 hours. Neuron-microglia co-cultures were pretreated with CpG for 3 hours before addition of 5 μmol/L oAβ1-42 for 24 hours. The supernatants of these cultures were collected. oAβ in 10-month-old-Tg 2576 mouse brain was extracted from the soluble, extracellular-enriched fraction as described previously.[21] Hemi-forebrains were harvested in 500 μl of solution containing 50 mmol/L Tris-HCl (pH 7.6), 0.01% Nonidet P-40, 150 mmol/L NaCl, 2 mmol/L EDTA, 0.1% SDS, and protease inhibitor mixture (Sigma-Aldrich, St. Louis, MO). Soluble, extracellular-enriched proteins were collected from mechanically homogenized lysates following centrifugation for 5 minutes at 3000 rpm.

Collected samples were mixed with sample buffer (200 mmol/L Tris-HCl, 8% SDS, and 1% glycerol). Proteins were separated on a 5 to 20% Tris-glycine SDS-polyacrylamide gel and transferred to Hybond-P polyvinylidene difluoride membrane (GE Healthcare UK, Buckinghamshire, UK). Membranes were blocked with 1% skim milk in Tris-buffered saline (TBS) containing 0.05% Tween20 (TBS-T). Blots were incubated in mouse anti-Aβ monoclonal antibody (6E10) (1/1000; Chemicon) diluted in 1% skim milk overnight at 4°C. Subsequently, membranes were washed in TBS-T 3 × 5 minutes and incubated with a horseradish peroxidase-conjugated anti-mouse IgG (1/5000; GE Healthcare) diluted in 1% skim milk for 1 hour. After washing in TBS-T for 1 × 15 minutes, 2 × 5 minutes, and TBS for 1 × 5 minutes, signals were visualized with SuperSignal West Pico Chemiluminescent Substrate (Thermo Fisher Scientific, Rockford, IL). The intensity of the bands was calculated by using CS Analyzer 1.0 (Atto, Tokyo, Japan).

Novel-Object Recognition Test in oAβ1-42-Induced Cognitive Impairment Mouse Model

oAβ (300 pmol/3 μl), CpG (100 nmol/L), or both oAβ and CpG were ICV injected as described previously.[22,23] The vehicle (PBS) was injected as the control. Briefly, a microsyringe with a 28-gauge stainless-steel needle 3.0 mm long was used for these experiments. C57/BL6 mice were anesthetized lightly with ether, and the needle was inserted unilaterally 1 mm to the right of the midline point equidistant from each eye, at an equal distance between the eyes and the ears and perpendicular to the plane of the skull. A single injection of 3 μl of peptide or vehicle was delivered gradually over 3 minutes. The injection site was confirmed in preliminary experiments. Neither insertion of the needle nor the volume of injection had a significant influence on survival and behavioral responses or cognitive functions.

The novel-object recognition test (NORT) was performed 7 to 8 days after ICV injection of oAβ1-42 or CpG as described previously.[24,25] The experimental apparatus consisted of a plexiglas open-field box (30 × 30 × 35 high cm), with a sawdust-covered floor. The apparatus

was located in a sound-attenuated room and was illuminated with a 60 lux light source. The NORT procedure consisted of three sessions: habituation, training, and retention. Each mouse was individually habituated to the box with 10 minutes of exploration in the absence of objects for 3 consecutive days (habituation session, days 4 to 6). During the training session, two novel objects were symmetrically fixed to the floor of the box, 8 cm from the walls, and each animal was allowed to explore in the box for 10 minutes (day 7). The objects were constructed from a golf ball, wooden column, and wooden triangular pyramid. They were different in shape and color but similar in size. An animal was considered to be exploring the object when its head was facing the object or it was touching or sniffing the object. The time spent exploring each object was recorded. After training, mice were immediately returned to their home cages. During the retention sessions (day 8), the animals were placed back into the same box 24 hours after the training session, but one of the familiar objects used during training had been replaced with a novel object. The animals were then allowed to explore freely for 5 minutes, and the time spent exploring each object was recorded. Throughout the experiments, the objects were used in a counterbalanced manner. A preference index in the retention session, a ratio of the amount of time spent exploring the novel object over the total time spent exploring both objects, was used to measure cognitive function. In the training session, the preference index was calculated as a ratio of the time spent exploring the object that was replaced by the novel object in the retention session over the total time exploring.

Cued and Contextual Fear-Conditioning Tests in Tg 2576 Mouse Model of AD

Cued and contextual fear conditioning tests were performed at 10 months of age according to previous report,[26] with minor modifications. For measuring basal levels of freezing response (preconditioning phase), mice were individually placed in a neutral cage (a block plexiglas box with abundant wood tips,30 × 30 × 40 high cm) for 1 minute, then in the conditioning cage (a transparent plexiglas box, 30 × 30 × 40 high cm) for 2 minutes. For training (conditioning phase), mice were placed in the conditioning cage, then a 15-second tone (80 dB) was delivered as a conditioned stimulus. During the last 5 seconds of the tone stimulus, a foot shock of 0.6 mA was delivered as an unconditioned stimulus through a shock generator (Neuroscience Idea). This procedure was repeated four times with 15-second intervals. Cued and contextual tests were performed 1 day after fear conditioning. For the contextual test, mice were placed in the conditioning cage, and the freezing response was measured for 2 minutes in the absence of the conditioned stimulus. For the cued test, the freezing response was measured in the neutral cage for 1 minute in the presence of a continuous-tone stimulus identical to the conditioned stimulus.

Stereotaxic injection was used for these experiments. Mice were anesthetized with sodium pentobarbital (50 mg/kg, i.p.) before stereotaxic implantation of a microinjection cannula into the right lateral ventricle (anteroposterior, −0.3 mm, and mediolateral, +1.0 mm, from the bregma, and dorsoventral, +2.5, from the skull according to the atlas of Franklin and Paxinos).[27] CpG was dissolved in PBS at a concentration of 10 or 100 nmol/L and was injected at a volume of 3 μl for 3 minutes. Same volume of PBS was injected to vehicle mouse. A week after injection, behavioral experiment was performed.

Immunohistochemistry

Immunohistochemistry was performed on brain tissue of mice after cued and contextual fear-conditioning test. Mice were transcardially perfused with ice-cold borate-buffered 4% paraformaldehyde under deep anesthesia. The brains were rapidly removed after decapitation. Brains were then postfixed overnight in periodate lysine paraformaldehyde, equilibrated in phosphate buffered 20% sucrose for 48 hours, and embedded into Tissue-Tek OCT compound (Sakura Finetechnical, Tokyo, Japan) and frozen at −80°C overnight. Coronal brain sections (20 μm) were cut with a cryostat. The sections were permeabilized with 1% Triton X-100 after blocking with 10% normal goat serum for 30 minutes. The cell nucleus was stained with Hoechst 33342 (1 μg/ml; Invitrogen). Aβ was stained with mouse monoclonal anti-Aβ antibody (4G8) (1/1000; Chemicon) and secondary antibodies conjugated to Alexa 488. Microglia were stained with a rat anti-mouse CD11b monoclonal antibody (1/1000; AbD Serotec, Oxford, UK) and secondary antibodies conjugated to Alexa 568. Images were collected and analyzed with a deconvolution fluorescent microscope system. Aβ load in immunostained tissue sections were quantified using BZ-analyzer (Keyence) as reported previously.[28] Seven sections were analyzed per animal. Total Aβ burden was quantified for the cortex and for the hippocampus on coronal plane sections stained with the monoclonal antibody 4G8. The cortical area was dorsomedial from the cingulate cortex and extended ventrolaterally to the rhinal fissure within the right hemisphere. Test areas (640 μm × 480 μm) were randomly selected. Total Aβ burden was calculated as the percentage of test area occupied by Aβ. Hippocampal measurements (600 × 600 μm) were performed similarly to the cortical analysis.

Statistical Analysis

Statistical significance of the biochemical experiments and the behavioral data were assessed with one-way analysis of variance, followed by post hoc Tukey test or Newman-Keuls test using GraphPad Prism version 5.0 (GraphPad Software, La Jolla, CA).

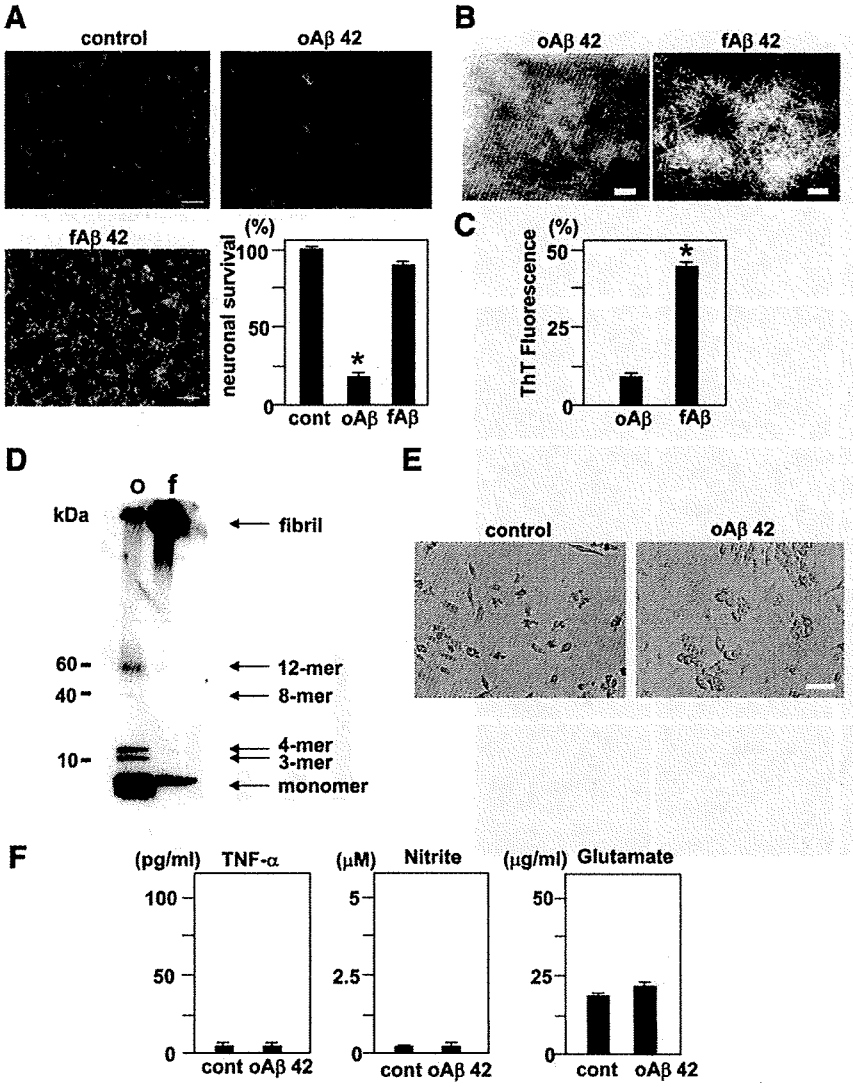

Figure 1. Neurotoxicity and morphologies of oAβ1-42 and fAβ1-42, and microglial response to oAβ1-42. **A:** The evaluation of neurotoxicity induced by oAβ1-42 and fAβ1-42. Neuronal cultures were treated with 5 μmol/L oAβ1-42 or fAβ1-42 for 24 hours. Neurons were stained with an anti-MAP-2 antibody (green). Aβ was stained with a mouse anti-amyloid β protein monoclonal antibody (4G8) (red). oAβ1-42 exhibited more striking neurotoxicity than fAβ1-42. Scale bar, 50 μm. Neuronal survival rate in oAβ1-42 treatment significantly decreased. $^*P < 0.05$ as compared with the rate in control cultures. Each column indicates the mean ± SEM ($n = 5$). **B:** Images of oAβ1-42 (**left**) and fAβ1-42 (**right**) collected with an electron microscope. Scale bar, 100 nm. **C:** Thioflavin T assay for oAβ1-42 and fAβ1-42. $^*P < 0.05$ as compared with the value of oAβ1-42. **D:** Western blot analysis of oAβ1-42 and fAβ1-42. oAβ1-42 (o) contained monomers, small oligomeric trimers (3-mer) and tetramers (4-mer), and the larger oligomers (octamers (8-mer) and dodecamers (12-mer)), whereas fAβ1-42 (f) contained monomers and fibrils. **E:** Microglial cultures were treated with or without 5 μmol/L oAβ1-42 for 24 hours. In a phase contrast, oAβ1-42 induced microglial adhesion. Scale bar, 50 μm. **F:** The measurement of TNF-α (**left**), nitrite (**middle**), and glutamate (**right**) produced by microglia activated with oAβ1-42. Microglial cultures were treated with 5 μmol/L oAβ1-42 for 24 hours. Each column indicates the mean ± SEM ($n = 7$).

Results

Neurotoxicity of oAβ1-42

First, we investigated the toxic effects of oAβ and fAβ on primary cortical neurons. Administration of 5 μmol/L oAβ1-42 to cortical cultures on DIV 13 for 24 hours resulted in significant neuronal death. The network of MAP-2-positive dendrites collapsed and neuronal survival decreased to 20% (Figure 1A). In contrast, administration of fAβ1-42 did not induce neuronal cell death, although Aβ deposition was observed on dendrites (Figure 1A). Thus, oAβ1-42 exhibits a more potent neurotoxicity than fAβ1-42. Both oAβ1-40 and fAβ1-40 did not induce neuronal cell death (Supplemental Figure S1, see *http://ajp.amjpathol.org*). We evaluated the morphology of oAβ1-42 and fAβ1-42 by transmission electron microscopy. We observed fine spherical particles of oAβ1-42 and fibril formation by fAβ1-42 (Figure 1B). The fluorescence of Thioflavin T, a marker for amyloid fibril formation, was associated with fAβ1-42 (Figure 1C). Western blotting with an antibody directed against Aβ (6E10) revealed that a solution of oAβ1-42 contained monomers, trimers (3-mer), tetramers (4-mer), and larger oligomers (octamers (8-mer) and dodecamers (12-mer)). In contrast, a solution of fAβ1-42 contained monomers and fibrils, but not oligomers (Figure 1D).

In primary microglial culture, administration of 5 μmol/L oAβ1-42 for 24 hours induced microglial adhesion (Figure 1E), but did not induce the production of neurotoxic mediators such as TNF-α, glutamate, or nitrite, a stable breakdown product of NO (Figure 1F).

Microglia Activated with CpG Attenuate the Neurotoxicity Induced by oAβ1-42

To define the role of microglia in the neurotoxicity of oAβ1-42, we evaluated neuronal survival in neuron-microglia co-cultures. Neurons stained with anti-MAP-2 antibody exhibited no detectable morphological abnormalities and possessed intact cell bodies and dendrites, and

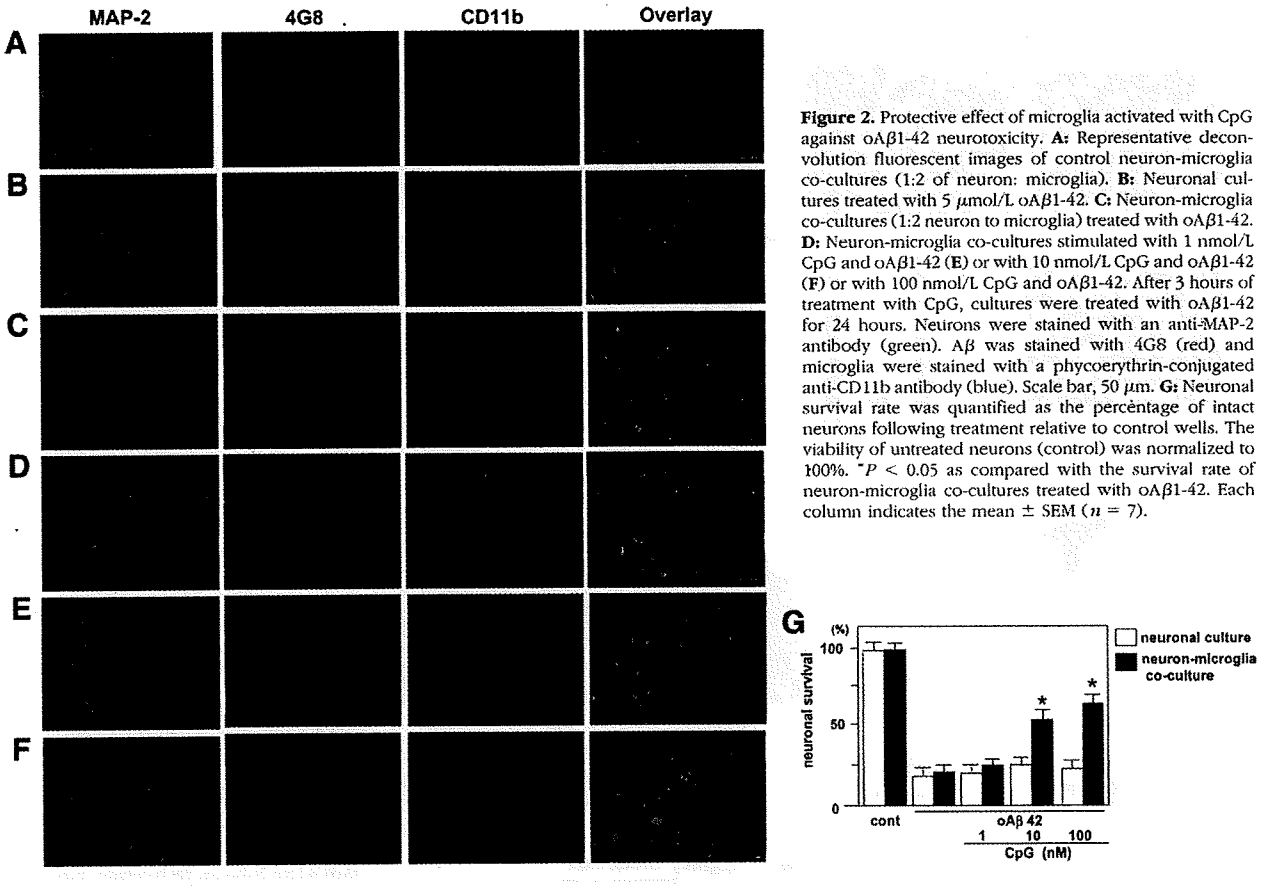

Figure 2. Protective effect of microglia activated with CpG against oAβ1-42 neurotoxicity. **A:** Representative deconvolution fluorescent images of control neuron-microglia co-cultures (1:2 of neuron: microglia). **B:** Neuronal cultures treated with 5 μmol/L oAβ1-42. **C:** Neuron-microglia co-cultures (1:2 neuron to microglia) treated with oAβ1-42. **D:** Neuron-microglia co-cultures stimulated with 1 nmol/L CpG and oAβ1-42 (**E**) or with 10 nmol/L CpG and oAβ1-42 (**F**) or with 100 nmol/L CpG and oAβ1-42. After 3 hours of treatment with CpG, cultures were treated with oAβ1-42 for 24 hours. Neurons were stained with an anti-MAP-2 antibody (green). Aβ was stained with 4G8 (red) and microglia were stained with a phycoerythrin-conjugated anti-CD11b antibody (blue). Scale bar, 50 μm. **G:** Neuronal survival rate was quantified as the percentage of intact neurons following treatment relative to control wells. The viability of untreated neurons (control) was normalized to 100%. $^{*}P < 0.05$ as compared with the survival rate of neuron-microglia co-cultures treated with oAβ1-42. Each column indicates the mean ± SEM ($n = 7$).

microglia stained with anti-CD11b antibody were also intact in unstimulated co-cultures (Figure 2A). After treatment of neuronal cultures with 5 μmol/L oAβ1-42 for 24 hours, the neuronal cells were severely damaged, and the survival rate decreased to 18% (Figure 2, B and G). Similarly, the neuronal survival rate was not improved in neuron-microglia co-cultures treated with oAβ1-42 (Figure 2, C and G), which implies that unstimulated microglia have not protective effect against oAβ1-42 neurotoxicity. Administration of CpG to neuronal cultures or neuron microglia co-cultures induced no toxic change (Supplemental Figure S2A, see *http://ajp.amjpathol.org*). After 3 hours of treatment with 1 nmol/L, 10 nmol/L, or 100 nmol/L CpG, 5 μmol/L oAβ1-42 was added to neuron-microglia co-cultures for 24 hours. The neuroprotective effect was not evident in culture with 1 nmol/L CpG (Figure 2, D and G). However, microglia treated with 10 or 100 nmol/L CpG prevented neuronal cell death, and the neuronal survival rate was significantly improved reaching 53 and 62%, respectively (Figure 2, E–G). In neuronal cultures, CpG did not attenuate the neurotoxicity induced by oAβ1-42 (Figure 2G). Moreover, 100 nmol/L CpG attenuated oAβ1-42-induced neurotoxicity for 48 hours, whereas other TLR ligands such as peptidoglycan and lipopolysaccharide did not (Supplemental Figure S2B, see *http://ajp.amjpathol.org*). We conclude from these findings that CpG-activated microglia have neuroprotective effect against oAβ1-42 neurotoxicity *in vitro*.

CpG-Activated Microglia Increase the Clearance of oAβ1-42, Produce the Antioxidant Enzyme HO-1 and Aβ-Degrading Enzyme MMP-9, and Release Fewer Neurotoxic Molecules

To elucidate the mechanisms of neuroprotection by microglia activated with CpG, we examined whether CpG increased the clearance of oAβ1-42. Western blot analysis revealed that there was no significant difference between the amount of oAβ1-42 present in the supernatants of neuronal cultures and in neuron-microglia co-cultures without CpG administration. (Figure 3A). However, CpG dose-dependently decreased the amount of oAβ1-42 in neuron-microglia co-cultures, especially treatment with 100 nmol/L CpG significantly decreased the amount of 3-, 4-, 8-, and 12-mer of oAβ1-42 (Figure 3, B and C). Moreover, we examined the effect of CpG on Aβ uptake by microglia alone at 1 and 24 hours time points. We found that CpG significantly enhanced microglial uptake of oAβ at both 1 and 24 hours (Supplemental Figure S3A, see *http://ajp.amjpathol.org*).

Because oxidative stress is a major component of oAβ1-42 neurotoxicity, we examined whether microglia activated with CpG express the antioxidant enzyme HO-1. CpG-activated microglia produced HO-1 in a dose-dependent manner. A total of 10 and 100 nmol/L CpG significantly increased the production of HO-1. The

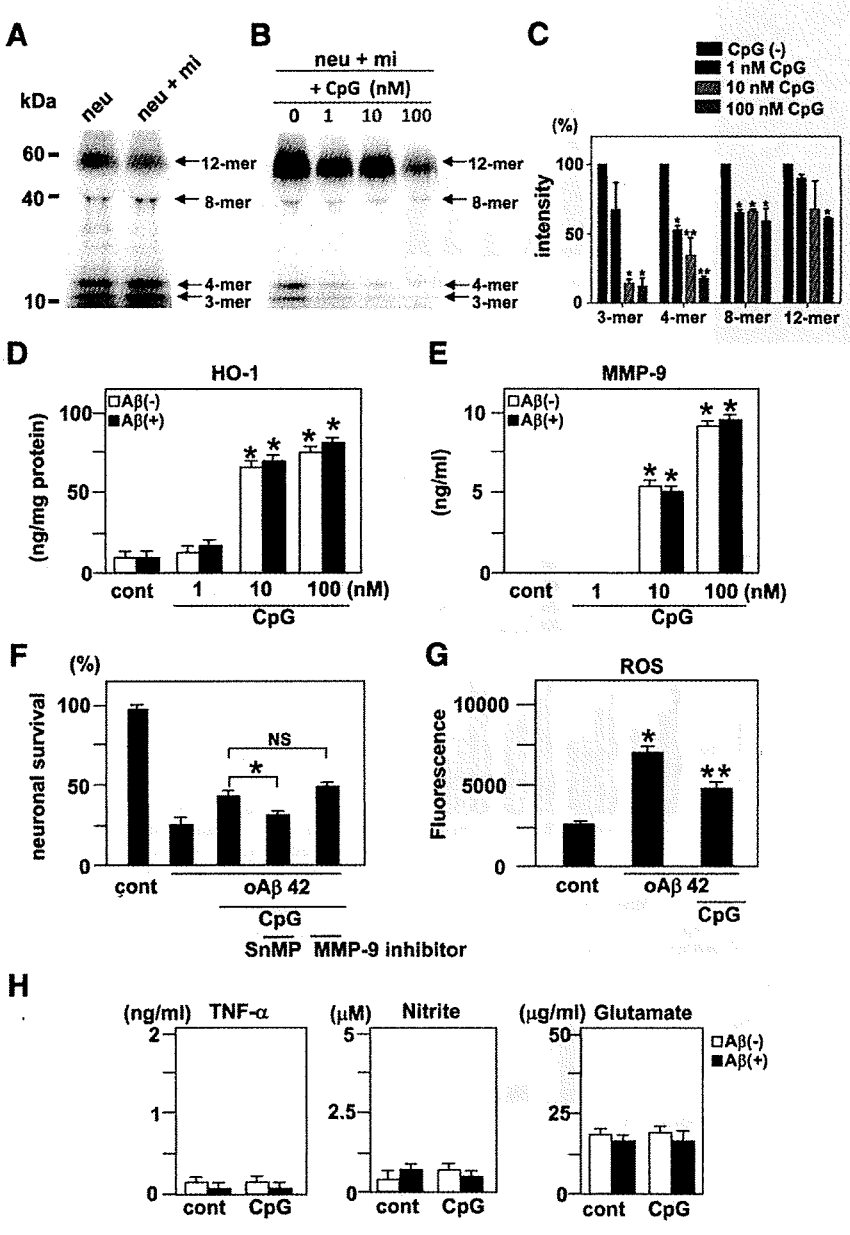

Figure 3. Clearance of oAβ1-42 and the production of HO-1, MMP-9, and neurotoxic molecules by microglia activated with CpG. **A:** Western blot analysis of oAβ1-42 in neuronal cultures (neu) and neuron-microglia co-cultures (neu + mi). Twenty-four hours after addition of 5 μmol/L oAβ1-42, oAβ1-42 present in the supernatants of these cultures was detected by Western blotting. **B:** Western blot analysis of oAβ1-42 in neuron-microglia co-cultures with CpG treatment. Neuron-microglia co-cultures (neu + mi) were treated with 5 μmol/L oAβ1-42 for 24 hours following 3 hours of treatment with 1, 10, or 100 nmol/L CpG. Microglia activated with CpG dose-dependently reduced the amount of oAβ1-42 in the supernatants. **C:** Semiquantification of oAβ1-42 in **B** by densitometric analysis. The amount of oAβ1-42 in neuron-microglial co-cultures without CpG (black) was normalized to 100%. oAβ1-42 in co-cultures treated with 1 nmol/L CpG (blue), 10 nmol/L CpG (green), or 100 nmol/L CpG (red) was calculated. $^{*}P < 0.05$ and $^{**}P < 0.01$ as compared with the intensity of oAβ1-42 in neuron-microglia co-cultures without CpG. Each column indicates the mean ± SEM ($n = 6$). The production of HO-1 (**D**) and MMP-9 (**E**) by microglia activated with CpG in the absence or presence of oAβ1-42. After 3 hours of treatment with CpG, microglial cultures were treated with or without oAβ1-42 for 24 hours. $^{*}P < 0.05$ as compared with untreated controls. Each column indicates the mean ± SEM ($n = 3$–5). **F:** The effect of HO-1 and MMP-9 on oAβ1-42 neurotoxicity. Neuron-microglia co-cultures were treated with 100 nmol/L CpG in the presence of 10 μmol/L tin-mesoporphyrin (SnMP) IX, a specific HO-1 inhibitor, or 50 nmol/L MMP-9 inhibitor for 3 hours, and then oAβ1-42 was added to the cultures for 24 hours. Tin-mesoporphyrin IX, but not the MMP-9 inhibitor, decreased neuronal survival rate. $^{*}P < 0.05$ as compared with CpG-treated cultures without inhibitors. Each column indicates the mean ± SEM ($n = 6$–9). **G:** The suppressive effect of CpG on ROS production by oAβ in the neuron microglia co-cultures. After neuron-microglia co-cultures were treated with or without 100 nmol/L CpG for 3 hours, cells were loaded with fresh nerve culture medium containing 5 μmol/L H_2DCFDA-AM for 30 minutes. After washing, culture medium containing 5 μmol/L oAβ1-42 was added and the increment of the fluorescence was calculated at 5 minutes. $^{*}P < 0.05$ as compared with untreated controls. $^{**}P < 0.05$ as compared with co-culture cells treated with oAβ1-42. Each column indicates the mean ± SEM ($n = 4$). **H:** The measurement of TNF-α (**left**), nitrite (**middle**), and glutamate (**right**) produced by microglia activated with 100 nmol/L CpG with or without oAβ1-42. After 3 hours treatment with CpG, microglial cultures were treated with or without oAβ1-42 for 24 hours. $^{*}P < 0.05$ as compared with untreated microglia. Each column indicates the mean ± SEM ($n = 7$).

production levels were not influenced by exposure to oAβ1-42 (Figure 3D). Since the anti-inflammatory cytokine IL-10 induces HO-1 expression by macrophages,[29] we also examined and confirmed that IL-10 induced HO-1 mRNA expression by microglia (Supplemental Figure S3B, see *http://ajp.amjpathol.org*). Although CpG induced IL-10 in microglia, the expression was suppressed by oAβ1-42 treatment (Supplemental Figure S3C, see *http://ajp.amjpathol.org*).

MMP-9 is also thought to play a neuroprotective role in AD because it degrades both oAβ and fAβ. A total of 10 and 100 nmol/L CpG significantly induced MMP-9 production in microglia with or without treatment of oAβ1-42 (Figure 3E). To determine whether HO-1 and MMP-9 contribute to the neuroprotective effects of CpG-activated microglia, we applied the specific HO-1 inhibitor tin-mesoporphyrin IX (Frontier Scientific, Logan, UT) and MMP-9 inhibitor (Merck, Darmstadt, Germany). The neuroprotective effect of CpG was abolished by treatment with 10 μmol/L tin-mesoporphyrin IX (Figure 3E). However, inhibition of MMP-9 with an MMP-9 inhibitor at 50 nmol/L did not influence the neuroprotective effect of CpG-activated microglia (Figure 3F). These results imply that HO-1 rather than MMP-9 may contribute to the

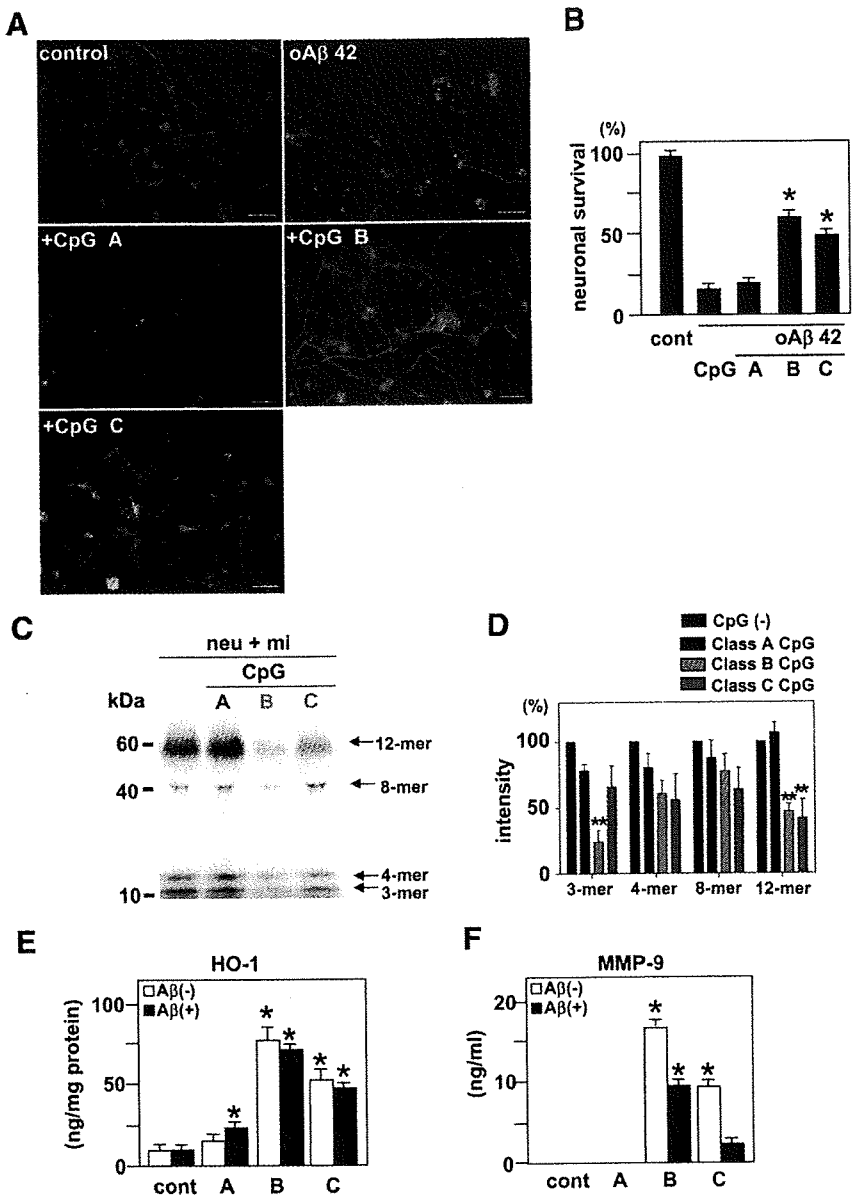

Figure 4. Protective effect of microglia activated with each subclass of CpG against oAβ1-42 neurotoxicity. **A:** Class B and class C, but not class A, CpGs exhibited neuroprotective effects against oAβ1-42 neurotoxicity in neuron-microglia co-cultures. After 3 hours incubation with 100 nmol/L class A, class B, or class C CpGs, oAβ1-42 was added to neuron-microglia co-cultures for 24 hours. Neurons were stained with anti-MAP-2 antibody (green). Aβ was stained with 4G8 (red), and microglia were stained with anti-CD11b antibody (blue). Scale bar, 50 μm. **B:** Neuronal survival rate was quantified. The viability of neurons in untreated co-cultures (control) was normalized to 100%. $^{*}P < 0.05$ as compared with the co-cultures treated with oAβ1-42 alone. Each column indicates the mean ± SEM ($n = 7$). **C:** Western blot analysis of oAβ1-42 in neuron-microglia co-cultures with subclassese of CpG treatment. Neuron-microglia co-cultures (neu + mi) were treated with 5 μmol/L oAβ1-42 for 24 hours following 3 hours of treatment with 100 nmol/L class A, class B, or class C CpGs. Microglia activated with class B or class C CpGs reduced the amount of oAβ1-42 in the supernatants. **D:** Semiquantification of oAβ1-42 in **C** by densitometric analysis. The amount of oAβ1-42 in neuron-microglial co-cultures without CpG (black) was normalized to 100%. oAβ1-42 in co-cultures treated with class A CpG (blue), class B CpG (green), or class C CpG (red) was calculated. $^{**}P < 0.01$ compared with the intensity of oAβ1-42 in neuron-microglia co-cultures without CpG. Each column indicates the mean ± SEM ($n = 7$). The production of HO-1 (**E**) and MMP-9 (**F**) by microglia activated with subclasses of CpG in the absence or presence of oAβ1-42. After 3 hours incubation with 100 nmol/L class A, class B, or class C CpGs, microglial cultures were treated with or without oAβ1-42 for 24 hours. $^{*}P < 0.05$ as compared with untreated control cultures. Each column indicates the mean ± SEM ($n = 3$–5).

neuroprotection of CpG. Furthermore, treatment of oAβ significantly increased ROS production in the neuron microglia co-cultures. Pretreatment of 100 nmol/L CpG significantly suppressed ROS production by oAβ (Figure 3G).

Although TLR4 ligand lipopolysaccharide generally increases microglial production of neurotoxic molecules including TNF-α, nitrite and glutamate; 100 nmol/L CpG did not induce these toxic molecules in microglia (Figure 3H).

Microglia Activated with Class B and C, but not Class A CpG, Attenuate oAβ1-42 Neurotoxicity

CpG ODNs are divided into three classes by their ability to induce IFN-α expression in plasmacytoid dendritic cells (class A) and to promote survival, activation, and maturation of B cells and plasmacytoid dendritic cell (class B) or both (class C)[30]. We examined which class of CpG induces the neuroprotective effects of microglia. Class A CpG neither activated microglia nor induced neuroprotective effects against oAβ1-42 toxicity, whereas both class B and C CpGs activated microglia and significantly increased neuronal survival, to 58 and 49% following oAβ1-42 treatment, respectively (Figures 4, A and B). Western blot analysis revealed that class B CpG significantly decreased the amount of trimers and dodecamers of oAβ1-42 present in the supernatants of neuron-microglia co-cultures, and class C CpG significantly decreased dodecamers of oAβ1-42, whereas oAβ1-42 did not decrease by the administration of class A CpG (Figure 4, C and D). In addition, microglia activated with class B and C CpGs expressed HO-1 in both the absence or presence of oAβ1-42, whereas treatment with class A CpG only slightly increased HO-1 expression in the pres-

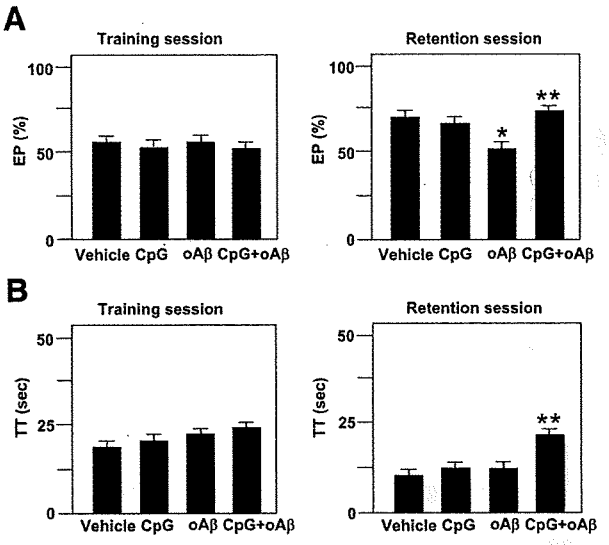

Figure 5. Effect of ICV injection of CpG on oAβ1-42-induced cognitive impairment in the NORT. **A:** Exploratory preference (EP) and total exploring time (TT) (**B**) in the training session (**left**) and the retention session (**right**). NORT was performed 7 to 8 days after ICV injection of oAβ1-42. Each column indicates the mean ± SEM (n = 6–7). $^{*}P < 0.05$ as compared with controls. $^{**}P < 0.05$ as compared with oAβ1-42-injected mice.

ence of oAβ1-42 (Figure 4E). Microglia activated with class B and C CpGs also produced MMP-9 (Figures 4F).

ICV Injection of CpG Ameliorates oAβ-Induced Impairment of Recognition Memory in the NORT

To examine the role of CpG-activated microglia in cognitive dysfunction induced by oAβ1-42, we investigated the effect of *in vivo* administration of CpG on the impairment of recognition memory in the NORT after ICV injection of oAβ1-42. Mice injected with oAβ1-42 displayed significantly reduced exploratory preference for the novel object in the retention session ($F_{(3,21)} = 3.68$, $P < 0.05$; Figure 5A), although total exploration time in the training and retention sessions was unaffected. The result implies that oAβ1-42 induces the impairment of recognition memory. Simultaneous injection of CpG with oAβ1-42 significantly improved both exploratory preference ($F_{(3,21)} = 3.68$, $P < 0.05$; Figure 5A) and total exploration time ($F_{(3,21)} = 4.41$, $P < 0.05$; Figure 5B) in the retention session, although exploratory preference and total exploration time were unaffected in the training session.

ICV Injection of CPG Ameliorates the Impairment of Associative Learning in the Cued and Contextual Fear-Conditioning Tests in Tg2576 Mice

Next, we examined the effect of CpG on the cognitive function of Tg2576 mouse model of AD. We evaluated associative learning at the age of 10 months in a conditioned fear learning test. In the preconditioning phase (training), the mice hardly showed any freezing response. There were no differences in basal levels of freezing response between the groups (data not shown). In the contextual learning test, wild-type mice showed a marked contextual freezing response 24 hours after fear conditioning (Figure 6A). However, vehicle-injected Tg2576 mice exhibited less of a freezing response in the contextual tests (Figure 6A), indicating an impairment of associative learning. The CpG (10 or 100 nmol/L)-injected Tg2576 mice were indistinguishable from wild-type mice, and the CpG treatment dose-dependently and significantly reversed the contextual freezing response as compared with vehicle-injected Tg2576 mice ($F_{(3,35)} = 9.54$, $P < 0.05$; Figure 6A). In the cued (tone) learning test, although there was no significant difference in the cued freezing response at 24 hours after fear conditioning between wild-type and vehicle-injected Tg2576 mice, both injection of 10 and 100 nmol/L CpG showed a tendency to reverse the cued freezing response (Figure 6B). No alterations of nociceptive response were found in any of the mutant mice: there was no difference in the minimal current required to elicit flinching/running, jumping, or vocalization among the mice (data not shown). Then, we examined whether CpG decreased Aβ deposits in the cortex (Figure 6C) and the hippocampus (Figure 6D) of Tg 2576 mice. No Aβ deposits were seen in wild-type mice. Although Aβ deposits (green) were abundant in the cortex and the hippocampus of vehicle-injected Tg2576 mice, ICV injection of CpG significantly decreased Aβ deposits in both areas. Microglia (red) clustered around Aβ deposits (Figure 6, C and D). CpG decreased Aβ load in a significant, dose-dependent manner in both areas (Figure 6E). We examined oAβ in the soluble, extracellular-enriched fractions of the hemi-forebrains of mice and detected 12-mer oAβ in vehicle-injected Tg2576 mice by Western blotting. The 12-mer oAβ was strikingly and significantly decreased in 100 nmol/L CpG-injected Tg2576 mice (Figure 6, F and G).

Discussion

Recent studies have proposed that oAβ1-42 contributes to the neurotoxicity associated with AD. AD begins with subtle alterations of hippocampal synaptic efficacy before frank neuronal degeneration, and this synaptic dysfunction is caused by diffusible oAβ.[31] Disruption of hippocampal long-term potentiation and synaptic plasticity by oAβ1-42 appears to involve Ca^{2+} signaling,[32] oxidative stress mediated by an *N*-methyl-D-aspartate receptor,[4,33] and protein phosphatase 1.[34] In addition, oAβ interferes with insulin receptor function in hippocampal neurons and inhibits the activation of specific kinases required for long-term potentiation.[35] In the present study, we have confirmed that oAβ1-42 exhibits more potent neurotoxicity than fAβ1-42 in murine cortical cultures.[5,36] Therefore, decreasing or preventing formation of oAβ1-42 is a potential therapeutic strategy against AD.

The precise role of microglia in oAβ1-42 toxicity remains unclear. Microglia stimulated with Aβ are reported to release proinflammatory cytokines via the nuclear factor κB[37,38] and contribute to the pathogenesis of AD. However, in our experimental conditions, oAβ1-42 neither